The Pennsylvania State University
The Graduate School

BLOCKAGE DETECTION IN NATURAL GAS PIPELINES BY TRANSIENT ANALYSIS

A Thesis in
Petroleum and Mineral Engineering
by
Najeem A. Adeleke

Submitted in Partial Fulfillment
of the Requirements
for the Degree of

Master of Science

May 2010

The thesis of Najeem A. Adeleke was reviewed and approved* by the following:

Michael A. Adewumi
Professor of Petroleum and Natural Gas Engineering,
Quentin E. and Louis L. Wood University Endowed Fellow
Thesis Co-Advisor

M. Thaddeus Ityokumbul
Associate Professor of Mineral Processing and Geo-Environmental Engineering
Thesis Co-Advisor

Turgay Ertekin
Professor of Petroleum and Natural Gas Engineering,
George E. Trimble Chair in Earth and Mineral Sciences,

Semih Eser
Professor of Energy and Geo-Environmental Engineering,

Yaw D. Yeboah
Professor of Energy and Geo-Environmental Engineering,
Head of the Department of Energy and Geo-Environmental Engineering

*Signatures are on file in the Graduate School.

Abstract

Pipelines are the most reliable means for the transportation of natural gas. A major problem of flow assurance in natural gas pipelines is solid deposition that result in partial/complete blockages. Blockages in natural gas pipelines are mostly due to hydrate formation and deposition. The industry has adopted a handful of hydrate formation prevention techniques however there is still no known means for the complete eradication of hydrates that is applicable under all pipeline blockage scenarios. The industry is now resorting to early blockage detection techniques in order to appropriately manage blockage scenarios for economic and safety reasons. Several studies have been conducted to determine the best approach for early blockage detection. Modeling and analyzing natural gas transients for blockage characterization is one of the promising early blockage detection techniques. It is the most economical and least intrusive simply because it requires no additional instrument other than a dynamic pressure gauge which is usually already part of most modern pipeline networks.

However, the problem with this technique lies in the resulting mathematical model. Its formulation results in a system of non-linear hyperbolic partial differential equations which have no known generalized solution. Besides, numerical techniques for solving the resulting mathematical model are computationally involved and are subject to numerical stability issues. This study explores the possibility of the use of a simple numerical technique based on finite volume method for blockage characterization.

In previous studies, pressure waves were assumed to be propagating at the speed of sound. This assumption is incorporated into the mathematical formulation by the isentropic assumption where the the pressure term within the momentum conservations flux is substituted for a function of the speed of sound. A calculated estimate of the speed of sound is then assigned prior to conducting numerical experiments. This assumption idealizes the model and causes the resulting pressure waves to propagate at sonic speed. The idealized solution and thereby affects the blockage characterization capability of the model when applied to real pipeline blockages or lab flow loop experiments. In this study, we do not make this assumption and instead the pressure one of our unknown variables. Hence the compression wave is expected to travels at its true speed.

Additionally, previous studies did not include viscous effects in their mathematical model for blockage characterization (Ahmed, 1996; Eltohami, 1999; Adewumi et al., 2000 and 2003; Chen et al., 2007). This is another assumption of ideality which further makes the solution impractical and reduces the accuracy of blockage characterization analysis. This study evaluates the effect of neglecting viscous effects on blockage characterization and a preliminary alternative equation

that accounts for the effect of friction on blockage severity estimation is proposed.

Furthermore, previous studies (Adewumi et al., 2000 and 2003) utilized empirical formulations (Dranchuk and Abou-Kassem, 1974) for the estimation of the compressibility factor. In this study, the mathematical formulation is a quasi-compositional Eulerian gas flow model in which the compressibility factor is estimated using the Peng-Robinson equation of state. This provides a more realistic prediction of transport properties since the composition of the gas is put into direct consideration.

The numerical techniques implemented here are specialized the for finite volume method of discretization. A staggered three-point stencil upwind scheme and a second-order centered five-point Nessyahu and Tadmor TVD scheme with MUSCL reconstruction are solved implicitly using the Newton-Raphson iterative technique. The fully implicit approach offers model stability for relatively large time steps thereby reducing the overall computational time despite the use of an iterative solver.

Blockage location prediction error was found to be reduced by one order of magnitude if the actual speed of the pressure wave that is determined from the inlet pressure profile is used. If viscous effects are considered, blockage severity analysis using the linear theory equation for determining wave reflection ratio that does not account for viscous effects results in large blockage severity prediction errors. However, blockage severity prediction is improved when the analysis is made in consideration of viscous effects.

Table of Contents

List of Figures

List of Tables

Acknowledgments

Indeed all praise is due to Allah, the creator of the universe and all that is in it. We praise him, and continue to seek his aid and guidance. I am most grateful to Allah, the exalted, through the commencement and completion of this work.The one without whom nothing is possible and with whom nothing is impossible.

I will like to show gratitude to Professors, Michael Adewumi and Mku Thaddeus Ityokumbul for their unwavering support and understanding through out the course of this work. Their continued support and understanding was instrumental to the success of this work and greatly appreciated.

Furthermore, I will like to show gratitude to all professors in Petroleum and Natural Gas engineering program for their nurturing courses and inspirations which set the pace of this development. Additionally, I will like to show gratitude to colleagues and well wishers in the department.

Finally, I will like to show gratitude to my parents, Alhaji Murtala S. Adeleke and Alhaja Muteaat T. Adeleke to whom I dedicate this work. Their love, encouragement and prayers were instrumental to the completion of this work.

Chapter 1

Introduction

Economic, technological, environmental and political drivers in addition to relative abundance have given natural gas its edge in the fossil fuel market today. Natural gas (NG) was flared for lack of economic viability in the past and preference was given to liquid hydrocarbons due to demand. However, this is no longer the case for several reasons. One reason is the hike in natural gas prices over the last couple of decades induced partly by the quest for energy independence by industrialized nations through control over the worlds' fossil fuel reserves. Another contributor to the appreciation of the value of natural gas is its clean burning attribute which appeals to environmentalist and proponents of global warming in both the developed and developing world. Additionally, the abundance of natural gas makes it appealing to energy policy makers who aim to enrich their portfolios with clean burning natural gas reserves to demonstrate their commitment to green energy supply. Furthermore, technological advancements in addition to the economic viability of natural gas makes deep water, tight shale and other unconventional natural gas reserves viable today. Notwithstanding, for natural gas to enjoy its increased demand it will have to maintain a competitive cost for consumers in the fossil fuel market.

One of the major impacts on the price of natural gas is its transportation. The quickest and most viable means of the transportation of natural gas is through pipe networks. Pipelines are a reliable avenue for the supply of NG to consumers. Another major impact on the price of this commodity is the cost of production. As more deep offshore developments emerge, the need to reduce risks associated with natural gas production is on the rise due to the large capital outlay associated with deep water developments. In such investments, time is money and lost time which can be caused either by temporary flow interruption or asset damage due to solid deposition greatly reduces profitability and therefore economic viability. Financial losses associated with flow assurance mishaps can be astronomical and hence the need to understand events associated with such mishaps.

Flow interruption may occur in pipelines due to partial blockages from condensation or solid formation and/or deposition. These may reduce deliverability hence making it difficult for gas

transmission companies to meet contractual obligations. In the least, partial blockages increase energy requirement for fluid transmission and thereby increases compression cost for gas transmission companies. Moreover, pipeline blockages could lead to catastrophic events such as pipe rupture in deep water developments. Solid deposition in pipelines may involve hydrates, paraffin wax, scale and naphthenates. For natural gas pipelines, most blockage occurrences involve gas hydrates. Hydrate deposition occurs after its formation under high pressure and low temperature conditions befitting of the deep water environments but not restricted to such. Figure 1.1 shows a generic hydrate equilibrium line which illustrates region hydrate formation. Hydrate deposition in NG pipelines are known to be the most catastrophic due to the possibility of complete pipe blockage. The Piper Alpha explosion incident is a tale much remembered in connection with such a fatal event. Remedial measures such as the use of hydrate inhibitors have not been able to completely eliminate the formation of hydrates and in fact effectively handling hydrate formation and deposition is one of the key aspects of flow assurance for NG systems.

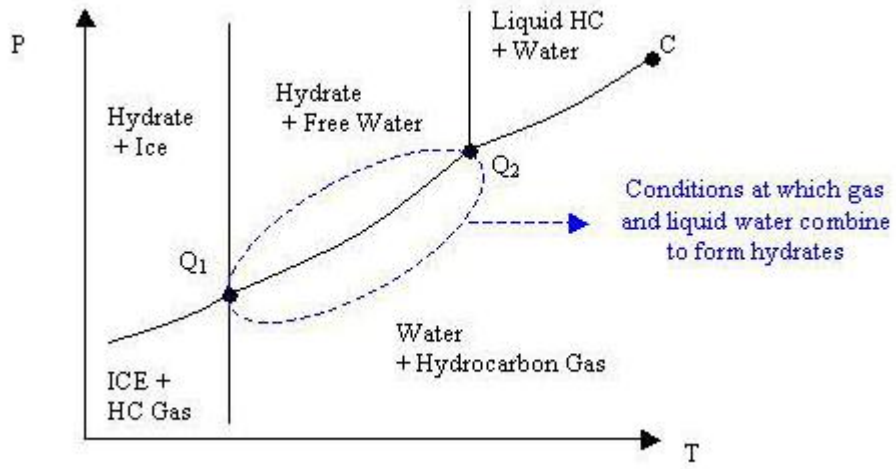

Figure 1.1: Generic Hydrate Formation Curve. *The properties of Petroleum Fluids (William D. McCain, 1990).*

The three-phase critical point is point C on the diagram that represents the condition where the liquid and gas hydrocarbon merge into a single hydrocarbon phase in equilibrium with liquid water. Point Q_2 is the upper quadruple point, where four phases (liquid water, liquid hydrocarbon, gaseous hydrocarbon, and solid hydrate) can be found in equilibrium. Point Q_1, the lower quadruple point, typically occurs at 32^oF (ice freezing point) where four phases (ice, hydrate, liquid water, and hydrocarbon gas) can be found in equilibrium.

The formation of hydrates can not be fully eliminated however early detection of solid depositions within pipes is one way to ensure flow and safety of people and assets. The knowledge of the location and severity of blockages in pipes will serve as a tremendous asset to NG transmission operators since it will help them to device optimum production schedules with the least possible

disruption during pigging operations. Additionally, it will help deep water operators maintain safety and integrity of deep water assets through early detection and remediation.

The goal of this study is to develop a transient, compositional gas flow model in order to explore the possibility of detecting the location and severity of partial blockages in pipes. Hydrate formation in pipelines have been reported to occur under the transient conditions of start-up or shutdown operations when pressure, temperature and fluid-property changes still exist. The advantage of the proposed techniques lie in the fact that it involves modeling transient states were hydrates are most likely to form and be deposited. The basic strategy is to use pressure transients to determine the existence of blockages in the pipeline. This transient is initiated by a surge in rate of fluid incursion into the pipeline that is allowed to propagate through the system. Upon reaching any obstacle transient reflections propagate back upstream to the inlet where pressure measurement are observed and blockage characteristic information are collected and analyzed.

Chapter 2

Background

2.1 Pipeline Blockages

Pipeline blockage may be structure-related or fluid-related. Structure-related blockages involves damage to pipeline infrastructure such as pipe deformation, valve malfunction and corrosion deposition which can all be avoided by proper maintenance and regular inspection. However, fluid-related blockages are more persistent and difficult to handle. Fluid-related blockages involve formation and/or deposition of solids such as asphalthenes and wax in oil pipelines and gas hydrates in natural gas pipelines. The most troublesome of these is gas hydrate deposition which is known to lead to catastrophic events. Hermmerschmidt (1934) was first to realize that it was gas hydrates and not ice that was plugging gas pipelines and ever since the main focus of flow assurance in natural gas pipelines has been effective handling of gas hydrates.

Natural gas hydrates are solid crystalline compounds resembling ice however much denser and form at temperatures above freezing point of water. They are formed by a non-chemical entrapment(enchlathration) of guest molecules in hydrogen bonded water crystal latices. These guest molecules are usually shorter chain hydrocarbons such as methane, ethane, propane and butane in addition to combinations of methane and other longer chain hydrocarbons. Other molecule such as nitrogen, carbon dioxide and hydrogen sulphide are also found in hydrates and are known to promote hydrate formation since they are more soluble in water than hydrocarbon. Hydrates are known to block transmission lines, plug blowout preventers, jeopardize the foundations of deepwater platforms and pipelines, cause tubing and casing collapse among other things.

2.2 Industrial Solutions

The key circumstances essential for hydrate formation are: (1) Presence of water (be it as a free phase or dissolved in another phase), (2) Hydrate conducive states i.e. low temperatures, high operating pressures and presence of short chain hydrocarbons (i.e. natural gas), (3) Turbulence

from high velocities, or agitation, or rapid pressure increase, or pressure pulsations (4) Presence of catalysts such as H_2S and CO_2. The solutions to the problem of hydrates hinges around the elimination of some of the above mentioned conditions or introduction of counter effect agents.

2.2.1 Chemical Injection

Though not the best approach, this is one of the most publicized method of handling the hydrate problem as it requires minimal interruption to gas flow and it is also less intrusive. Just like the presence of H_2S and CO_2 promotes hydrate formation because both of these acidic gases are more soluble in water than the hydrocarbon, other chemicals may be introduced into natural gas transmission lines to induce the opposite effect. These chemicals inhibit the formation of hydrates by shifting the hydrate formation line of equilibrium (see Fig. 1.1).

Hemmerschmidt(1934) conducted early studies on hydrate inhibition using aqueous solutions such as lithium chloride, calcium chloride, zinc chloride, di-ethylene glycol, methanol and glycerine. Nakamaya and Hashimoto (1980), Davidson et al. (1981), Makogon(1981), Berecz and Balla-Achs(1983), Svatar and Fadnes (1992), Kelland et al. (1995) also have all conducted similar studies. More recent studies have been on the mechanisms of gas hydrate inhibition. See Sloan (1991), Lederhos et al.(1996), Sloan (2003). Though these studies have greatly increased our understanding of gas hydrates, there is still no known hydrate inhibitor that can completely eliminate the problem of hydrate formation and deposition.

The two most common hydrate inhibitor used today are methanol and ethylene glycol. However, methanol injection continues to be the most simple and cost effective inhibition agent. It is most beneficial in cases where hydrate problems are relatively mild, infrequent and in cases where inhibitor injection is only a temporary phase, or where inhibition is done in conjunction with a primary dehydration system as will be discussed later. Hence the need for alternative measures to curb the problem under more severe conditions still exists.

2.2.2 Natural Gas Dehydration (Water Dew point lowering)

No hydrate formation is possible if water is not present hence we understand the importance of removal of water vapor from natural gas systems. Removal of water from natural gas causes hydrate instability since the host molecules (water) become insufficient to form enough lattices to house the guest molecules. This is the only method so far found to be completely satisfactory in preventing the formation of hydrates in transmission lines. It is important to mention that a common misconception is that for the formation of hydrate, water must exist as a "free" phase. However, from a strictly thermodynamic point of view, vapor or liquid hydrocarbon with dissolved water can form hydrates at the hydrate-vapor or the hydrate-liquid hydrocarbon (HC) boundaries with out the presence of a free water phase (see Fig.2.1)

Figure 2.1 shows the cooling of a 60 mol percent CH4 + 40 mol percent H_20 mixture from a high temperature at a constant pressure shown as a dashed vertical line. The vapor (v) exists as a single phase until the water dew point (Point 1) is reached, where composition of equilibrium

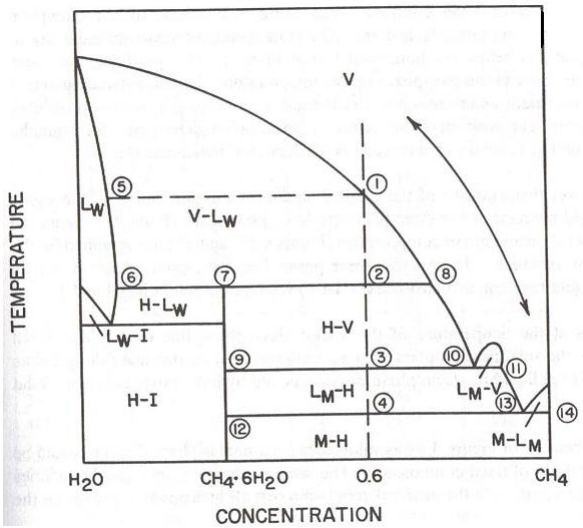

Figure 2.1: Temperature-Composition diagram for Mehtane and Water. *Clatherate Hydrates of Natural Gases, (Dendy E. Sloan, 1998)*

liquid water (Lw) is point 5. Further cooling of the gas-liquid mixture causes the water phase to increase until point 2 (Lw-H-V coexists) is reached where hydrate (H) phase forms. Note that if at point 8 hydrate phase forms from the vapor phase and if at point 6 hydrate phase forms from "free" water phase. Further reduction in temperature results in the conversion of any available free water to hydrate and the system enter a two phase (H-V) region below horizontal line at point 2. Further reduction in temperature causes some of the methane in the vapor phase to transition into liquid methane (Lm) at the three phase (Lm-H-V) boundary. Further reduction in temperature results in the conversion of any available methane in vapor phase to liquid methane and the system enter a two phase (H-Lm) region below horizontal line at point 3. point 4 is the point of the lowest three phase (H-Lm-Sm) line where solid methane (Sm), liquid methane and hydrate exists in equilibrium. A further reduction in temperature causes the conversion of all available liquid methane in solid methane below the horizontal line at point 4. Hence only solid phase methane and hydrate exists below this temperature.

After free water is separated from the gas stream, Figure 2.1 shows the need to remove water present in both the liquid and vapor hydrocarbon phases. Within ten years of Hammershmidt's 1934 discovery of hydrates in pipelines, he and his colleagues published details of gas dehydration with solid dessicants. The most common solid desiccants today in order of decreasing drying efficiency are molecular sieves, silica gel and alumia. Molecular sieves are crystalline solids designed to adsorb particular molecules based upon polarity and size. They have become the dominant absorbent due to the advantages of extremely low due point, high water adsorption capacity and unlike silica gel are not damaged by liquid water.

Deaton and Frost (1946, p.42) suggested three processes for dew point lowering removal of dissolved water: (1) Hygroscopic solution (2) Chemical adsorption (3) Physical adsorption by

solids. Of the three suggestions only two have evolved into commercial processes. The third process we already discussed. The second process is not in commercial use based of the economic feasibility of the use of non-regenerative solid chemical adsorbents. However, the first involves lowering the water concentration by contacting the gas with tri-ethylene glycol (TEG) which adsorbs water through hydrogen bonding. Detailed description of this process can be found in Perry (1960), Hall and Polderman (1960), Loomer and Welch (1961) and Bucklin et al. (1985).

As mentioned earlier, water removal is one of the most satisfactory approach to preventing hydrate formation. However, other than the fact that it increases the overall cost of transportation of natural gas, it requires a technical process which may not always be practically implementable. For instance, in deep water production of natural gas, hydrates formation occurs before one ever gets the natural gas to the surface. In such cases the dehydration process can not be implemented.

2.2.3 Maintenance Operations

2.2.3.1 Optimal Transmission Operations Design

Since hydrate inhibitors can not completely eliminate hydrate formation and deposition transmission operators have been able to use the knowledge of hydrate forming conditions to optimize gas transmission operations to reduce hydrate formation in transmission lines when possible. Hydrates occur at or below the hydrate formation temperature for a given pressure and gas composition. Phase behavior thermodynamics is usually invoked for the prediction of the lower and upper quadruple points (Q1 and Q2) on the hydrate formation/dissociation line (see Fig. 1.1).

The first two methods of prediction were proposed by Katz and coworkers, and are known as the Gas Gravity Method (Katz, 1945) and the Ki-value Method (Carson and Katz, 1942). Both methods allow calculating the Pressure-Temperature equilibrium curves for three phase systems involving liquid water, hydrate and natural gas. These methods yield initial estimates for the calculation and provide qualitative understanding of the equilibrium; the latter method being the more accurate of the two. See Sloan (1990) for more detail. The third method relies on Statistical Mechanics for the prediction of equilibrium. It is recognized as the most accurate of all three-phase calculations as it is more comprehensive and detailed.

2.2.3.2 Regular Pipe inspection and Pigging Operations

One good but intrusive method for removing hydrates from pipelines is pigging. The industry has adopted pigging as a remedial measure and most pipeline networks are constructed with pig lunchers and receivers built on with bypass and isolation valves that allow fluid to either flow through or around the pig launcher/receivers. Also ball valves instead of butterfly valves are used to accommodate pig trafficking through pipelines. Pigging is the practice of inserting a device known as the "pig" into a flowing pipeline. Pig devices vary depending on usage. They may be used to scrape off solid deposits (hydrates, wax, paraffins) from the inside of the pipeline, or to

remove liquids and condensate from NG pipelines. Pigs can also be used to inspect the pipeline for corrosion damage, leakages or for blockage detection.

Pigs for cleaning may be as simple a polyurethane foam plug to push along liquids and condensates or include tungsten studs with abrasive wire meshes on the outside to cut rust, scale or paraffin. Pigs used for inspection, also known as "smart pigs" or "intelligent pigs", are highly sophisticated instruments that vary in complexity based on the intended usage. Magnetic Flux Leakage (MFL) pigs are smart pigs used for surface pitting and corrosion inspection as well as cracks/weld defects. Caliper pigs on the other hand are a much simpler type of smart pigs used for determining roundness of the pipeline.

The pig diameter is bigger than the pipe diameter so the pipe is sealed on both sides and driven by gaseous or liquid propellants or whatever fluid is in the pipe at the time. Pigging helps keep the pipeline free of liquids and solid deposits, reduce the overall pressure drop and increase pipeline flow efficiency. However, pigging operations are associated with a great deal of risk which can be very costly. The risks range from mechanical failures to safety issues. One problem associated with pigging operations is the possibility of the pig getting lodged behind an obstruction within the pipe. Not only is it costly to locate and retrieve the pig, usually done by a contractor firm specializing in pig retrieval, it is also an obstruction to the production schedule.

A whole industry thriving off of the eminent need for pig retrieval services have emerged. This services are mostly needed in the early stages of operation when not much is known about the interior of the pipe which therefore increases the risk of having a stuck pig. The risks associated with pipeline pigging highlights the need for non-intrusive methods for locating and determining the severity of pipe blockages.

2.2.4 Early Blockage Detection Techniques

2.2.4.1 Blockage Detection Using Acoustics

Acoustic techniques were formally used for leakage detection in pipelines. Prior to this, bar test surveys were used to detect leakages in natural gas transmission lines. Bar test surveys also known as "barholing" are carried out by driving or boring bar holes at regular intervals along the way of an underground gas pipe line and the atmosphere in the holes is tested with a combustible gas detector or similar equipments. This was the standard method and is still in use till today. The first attempts to develop methods for leak detection using acoustics appeared in the 1930's (Parker, 1981). Smith (1933); Gilmore (1935); Richardson (1935) and Larson (1939) all had publications on acoustic techniques in the same decade. However, there were no more publications on the subject for another two decades (McElwee, 1957).

Earlier studies were based on a passive approach in the sense that they limited the technique to the use of listening devices. Sonic Sensors were coupled to the gas stream inside the pipe and since noise generated from leakage is distinctly audible and renders ambient noise negligible, leakage detection was possible. However, in the late 50's to the mid 60's the Institute of Gas Technology(IGT) with the support of The American Gas Association (A.G.A.) made record

progress in the first systematic attempt to develop an improved approach using both passive and active acoustic techniques for leak detection (Reid, 1961 and Hogan, 1964). Although IGT achieved some success in leak detection at the time, the systems developed were not considered reliable enough to replace the traditional bar test surveys.

The theoretical and experimental work in this area was unraveled by Parker (1981) who identified factors of major importance in the operation of active leak detection systems. He developed a correlation to improve signal to noise ratio that was independent of time, hence very small initial values of emitted acoustic signals could be detected even after relatively long periods of time with damping effect. The pitfall of his acoustic technique was in its limited application to sensors in close proximity to the leak site thereby requiring a mobil sensor to traverse the pipe. Hence continuous monitoring was not feasible.

In the late 80's Watanabe and his coworkers introduced a new acoustic leak detection technique where a leak in the pipeline was estimated by impulse response to an acoustic wave from signals detected at two terminal sites within a pipe. This method requires continuous monitoring through microphones at both the input and output terminals and is based on the observation that sudden leaks in pipes produce sharp impulse responses to acoustic waves. Watanabe's modeled a pipeline like a tube wind instrument with resonance and standing waves computed as a function of leak position (Watanabe et. al. 1986, 1987a, 1987b, 1990) by introducing "white noise" a distance from the leakage site at the input terminal and acoustic signals excited by the white noise are detected at both terminals. It is important to note that Loth, et. al. (2003) developed a theoretical model of the wave equation to show how and why the leaks could be detected using Watanabe's model. Watanabe's model was based on the following initial assumptions:

1. the test zone in the pipe system has two constrictions, one at the input end and one at the output end,
2. the pipe system is a single tube with no side branches,
3. there can only be one leak in the test section at one time (this was only an initial assumption and the application of this technique to multiple leakages can be demonstrated where time locations are derived (Loth, et. al., 2003)),
4. the entire test section has a uniform cross section,
5. the pressure at the input end includes random, almost white, fluctuations,
6. the pressure at the input and output can be measured with a microphone having a limited frequency range, and
7. the acoustic wave propagates through the pipeline without attenuation and the velocity of the fluid in the pipe is insignificant when compared to the speed of sound.

Koyama et. al. (1993) extended Watanabe's studies to include the detection of blockages and blockage severity in pipelines with the following assumptions:

1. The fluid in the pipe is ideal gas
2. There is only one blockage in the pipe
3. The tested zone is a straight section of pipe with no branches and bends
4. The tested zone has a uniform cross-section in the absence of partial blockage
5. The outlet of the pipeline is partially closed

The advantage of this method is that it can be used to detect both blockages and leakages. However, this technic requires that both the inlet and outlet be fitted with microphones which further complicates the design of the pipe network. However, the main disadvantage of acoustic methods in general is the degradation of acoustic signals.

Another acoustic method that can be used to detect blockages as well as leakages was proposed by Sharp and Campbell(1996). They discussed a method involving the injection of sound pulse into a pipeline and recording of resulting reflections using a microphone installed on the exterior of the pipe. The premise of this method is from the idea that for an ideal delta function sound pressure pulse, the reflection obtained from the pipe should be its input impulse response. However, lack of ideality causes a deviation in the impulse response reflections. The reflections obtain are deconvolved using the input pulse to obtain the impulse response using Fourier transforms. Analysis of this reflection is used to obtain information about the bore profile as well as the input impedance of the pipe.

2.2.4.2 Blockage Detection Using Pressure Transients

Transient modeling have been used to study several problems in the natural gas industry ranging from the determination of pressure drop and flow rate of natural gas at different nodes in a pipe network undergoing variations in demand and supply, to the analysis of compressor start-up and shut-down operations. Ratchford and Dupont (1974), Stoner (1969), Wilkinson et al. (1965), Steeter and Wylie (1970), Thompson and Skogman (1983) all are examples of transient modeling in the natural gas industry. The last paper applies transient fluid flow and heat transfer models to real time pipeline leak detection.

Transients are in general a short-lived phenomena that can be observed over a finite period of time prior to the system achieving steady or pseudo-steady conditions. Transients are studied not only in fluid flow but also in electrical circuits, mechanical system deformation, and even astronomy. Transient analysis of natural gas systems involves the solution of a system of non-linear partial differential equations with initial and boundary conditions. The fact that there is no generalized solution for non-linear PDEs highlights the difficulty involved in solving this problem. The starting point in formulating most mathematical models involving fluid flow is the Navier-Stokes equation. Solving such an equation is never an easy task and always involves compromises. Moreover, the Navier-Stokes equation is simply a statement of momentum conservation and in order to adequately describe the flow of fluids, more information is needed depending on how

much justifiable assumptions are made. However, regardless of assumptions made, a statement of the conservation of mass (or the mass continuity equation) is generally necessary.

The earliest solution for partial differential equations was given by Jean le Rond D'Alembert in 1750 in application to a vibrating string. It is a simple algebraic method requiring excessive assumptions. It should be noted that Bernoulli also came up with a very different solution in the same year based on eigenfunction comparable with the Fourier series and this forms the basis for numerical Fourier transforms in the field of electrical engineering today. The concepts and theory of transients have been well developed since D'Alembert's solution starting with Alleivi(1902) who first applied the theory to the field of hydraulics and established the general theory and the idea of a graphical method. However, since the advent of digital computers these methods have become obsolete and are only referenced for chronographic or pedagogic reasons. Schnyder (1929), Bergeron (1935) and Angus (1935) applied Alleivi's graphical method to analyze the water hammer phenomena. This method is known today as Bergeron's method in the field of electrical engineering though it was first developed by Schnyder. The water hammer phenomena is synonymous to line packing effect in natural gas systems.

Computer advancements have made more accurate methods that were previously considered too costly due to their heavy computational loads more prominent today. Hence, the old conventional wisdom that resulted in simplification of mathematical formulations is no longer necessary. Now the criteria are practicalilty/accuracy and computational time cost. These two need to be juggled carefully to arrive at an optimum model by minimizing computation time without compromising the physical integrity of the model. The field of numerical analysis is very broad and divided into various aspects depending on the type of problem that needs to be solved. For differential equations, a solution is reached through (1) Development of a mathematical model that describes the physical problem (2) Identification of the domain of the mathematical formulations, (3) Discretization of the differential equations involved into a finite dimensional subspace, (4) Application of a numerical scheme and appropriate treatment of boundary condition(s), and (5) Application of a numerical solver.

Computational mathematical models usually involve differential equations. Differential equations vary across one or more domain which must be discretized. Discretization can be done by finite difference, finite element, finite volume, and so on. In this study we will be using finite volume since it is a conservative discritization technique and is expected to yield better results in comparison to alternative options for the conservation laws. After descritization, a numerical scheme is formulated to represent the original mathematical formulation in a finite domain. A solver is then applied to the numerical scheme to obtain approximate solutions to the physical problem described by the mathematical formulation. In this study we will be comparing several numerical schemes and an iterative solver will also be utilized to obtain simultaneously the solution of every cell within our finite domain.

The numerical technique to be used is influenced by the mathematical formulation of the problem to be solved. The method of characteristics (MOC) is known to be one of the best methods for solving first-order hyperbolic partial differential equations though it can be used to

solve any PDE. MOC simplifies the system of hyperbolic PDE describing gas flow by converting them to ODEs integrated along the natural co-ordinates of the system otherwise known as the characteristics. The resulting characteristic equations obtained can be solved numerically on either a grid of characteristics or on a rectangular coordinate grid. The disadvantage of MOC is that it is comparatively slow since the time steps are strictly restricted by the stability criterion. Issa and Spalding (1972) and Wylie et al. (1974) both used the method of characteristics to solve transient one-dimensional flow. Wylie applied the inertia multiplier in a pipe network model as proposed by Yow (1972). It was found that the time step size could be adjusted to the desired degree of accuracy to suit the particular transient that is being imposed upon the system and arbitrary pipe lengths may be treated without awkward adjustments to satisfy the common time interval requirements of the Courant-Friedrichs-Lewy (CFL) condition (Wylie et al., 1974).

Ratchford and Dupont (1974) used the Galerkin method to simulate two-dimensional isothermal transient gas flow. They multiplied the set of hyperbolic PDEs by a restricted set of continuous real functions (Hermite cubic polynomials) on uniform spacing along the length of the pipe before integrating in space to obtain a new set of non-linear ODEs. The system of non-linear ODEs were then discretized in time using finite difference method to second order accuracy and solved implicitly.

There are many first and second order, explicit and implicit numerical schemes applicable to finite difference discretization. Heath and Blunt (1969) used a finite difference method known as the CrankNicolson method to solve the conservation of mass and momentum equations for slow transients in modeling isothermal gas flow. It was found that this method does not always give a stable solution according to the Neumann stability analysis of large time steps for nonlinear problems. Wylie et al. (1971) also presented an implicit central finite difference scheme and compared it with the method of characteristics. They showed that implicit methods are accurate for large time steps and are not limited by the stability criterion of the MOC.

Poloni et al. (1987) used an explicit Lax-Wendroff scheme which is second-order accurate with finite difference discretization and they found that first-order finite difference schemes are not sufficiently accurate for modeling gas transients in pipelines. Kiuchi (1994) used a fully implicit finite difference scheme to model transient isothermal compressible flow and compared it with MOC, LaxWendroff method, Guys method, and CrankNicolson method. It was found that the fully implicit finite difference scheme is unconditionally stable if the inertia terms in the momentum equations are neglected. Like Wylie (1971), they also found that the fully implicit schemes are accurate for large time step sizes.

Zhou and Adewumi (1995, 1996) developed a one-dimensional isothermal transient gas flow model without neglecting any terms in the conservation of momentum equation using a monotone preserving finite difference scheme having the property of a Total Variation Diminishing (TVD) scheme by introducing a 'limiter' which controls the gradients of the computed solution so as to prevent the appearance of any over/undershoot as first introduced by Harten (1983). The results were compared to the first-order Godunov scheme and it was found to be better suited for the problem. Ibrahim and Adewumi (1996a, 1996b) also implemented an upwind finite

difference TVD flux splitting scheme developed by Steger/Warming and its modification by Van Leer as well as that proposed by Roe. The 4th order Runge-Kutta method was used along with the spacial TVD scheme to achieve higher-order temporal resolution. Adewumi et al. (2000 and 2003) also used the TVD scheme to model a one-dimensional isothermal non-compositional single-phase Eulerian model to describe the propagation of a pressure pulse through a pipe with multiple blockages. They demonstrated the possibility of detecting multiple blockages in pipelines by monitoring and analyzing pressure variations at the inlet caused by reflections of the propagating transient in order to deduce the internal configuration of the pipe. Their work is of pivotal importance to this study.

Although Adewumi et al. (2003) included viscous effects in their model, they neglected it in order to properly characterize the blockages using the inlet pressure profile. Hence, instead of the experience of a slow but continuous increase in their inlet pressure profile over time due to frictional force deterring flow. Their inlet pressure profile instead showed a constant value after the initial increase induced by the imposition of a constant mass flux passing through the system. In this study, we will be exploring the possibility of achieving blockage detection without neglecting viscous effects. Additionally, their numerical technique requires relatively large computational time due to smaller time step requirements as a result of stability restrictions. Moreover, the numerical technique is also highly computationally involved. In this study we will explore the possibility of using a simpler less computationally involved numerical technique while maintaining physical consistency of the mathematical model. We will also make use of a numerical technique whereby we will solve the system of equations implicitly in order to maintain accuracy of the solution for relatively large time steps and improve stability. The system of equations will also be solved simultaneously for every grid cell in order to reduce computational time.

Chen et al. (2007) also explored the feasibility of blockage detection using transient simulation of an isothermal Eulerian model. They cited and implemented the TVD scheme presented by Zhou and Adewumi (1996). They also cited the work of Adewumi et al. (2000 and 2003) and utilized the analytical solution for the analysis of the inlet pressure profile adopted from linear theory. The inlet pressure analysis technique was also applied to experimental inlet pressure data collected by a dynamic pressure gauge on a flow loop. For the numerical experiments, blockage location and length prediction errors were found to be within $\pm$ 5 % and blockage severity prediction error was found to be under $\pm$ 3 %. For the single phase flow loop experiment, blockage location and length prediction errors $\pm$ 0.02 % and $\pm$ 0.5 % respectively, while blockage severity prediction error was under predicted by 48 %.

Adewumi et al. (2000 and 2003) and Chen et al. (2007) both incorporated the speed of sound in their mathematical description of the single phase fluid flow problem by assuming the compression/pressure wave is an acoustic wave (See Hirsch, 2007 [2nd Edition]). Therefore it is expected that the compression wave generated in their studies will propagate at the speed of sound. In this study, the pressure value within the flux term of the momentum equation is one of taking as one of the unknown variables obtained iteratively. Therefore, compression wave generated are expected to propagate at its actual speed. It is intuitive that the speed

of a compression wave will differ from that of sound wave propagation base on the fact that sound waves propagate within a medium as a result of the vibration of particles/molecules while pressure waves propagates as a result of compression or expansion involving every molecule along a path within a medium.

2.2.4.3 Blockage Detection Using Steady State Techniques

For the sake of completeness we will discuss another set of early blockage detection techniques available in the literature. Information necessary to implement these techniques must be collected under steady state conditions in order to ensure accuracy. This methods are also referred to as Frictional loss methods and have been successfully tested in laboratories to detect changes in pipe diameter, hence an indication of blockage severity. However they are neither recognized for determining blockage location nor for multiple blockage detection.

2.2.4.3.1 Blockage Detection Using the Backpressure Technique Cullender (1955) and Fetkovich, (1975) applied the backpressure technique for inflow performance monitoring in gas wells. When applied to gas pipelines, this technique provides a means of monitoring flow performance. A baseline is established based on the premise that a linear relationship is expected between flow rate and the difference of the square of the pressure at the inlet and outlet of a pipe under steady state conditions. Therefore, plotting flow rate versus ΔP^2 should yield a straight line. Deviations from this is then an indication of leakages/blockages along the pipe. Scott and Satterwhite (1998) applied the backpressure technique gas pipelines for blockage detection and attempted to quantify the deviations through the introduction of a blockage factor for both "fully rough" pipe and "smooth" pipe defined based on pipe friction factor determination. The difficulty in utilizing this method lies in the establishment of the baseline which requires a multirate test.

2.2.4.3.2 Mass Balance Technique The mass balance technique relies on the fact that matter is always conserved. Thus accurate metering of all materials entering and exiting from the inlet and outlet of a pipe under steady state condition is required and expected to tally up. Deviations indicate either leakage. Longer flowlines and the limited ability to accurately meter flowrates further reduces the feasibility of this technique in determining blockage location and severity.

Chapter 3

Mathematical Formulation

The complete representation of any transfer process can be derived from the general transport equation below. The generic scalar transport equation is a general PDE that describes transport phenomena, or better still, the mechanisms by which particles or quantities move from one place to another.

$$\frac{\partial \phi}{\partial t} + \nabla \cdot f(t, x, \phi, \nabla\phi) = g(t, x, \phi) \tag{3.1}$$

The earliest works in fluid dynamics dates back to medieval Persian and Arab natural philosophers. From the likes of polymath scientist Abu-Rayhan Al-Biruni (973-1048) who was the first to apply experimental scientific methods to mechanics. He established the experimental methodology for the determination of weight per unit volume of matter (or specific weight). Physicists like Al-Biruni and Al-Khazini (1115-1130) who also designed the first hydrostatic balance, unified statics and dynamics into continuum mechanics. Their achievements were complimentary to the works of their predecessors such as Al-Farabi (872-950), Aristotle (384BC-322BC) and Archimedes (287BC-212BC) who mostly focused on static mechanics. Later between the 15th to 18th century came European scientists of the likes of Leonardo da Vinci (1452-1519), Evangelista Torricelli (1608-1647), Blaise Pascal (1623-1662), Isaac Newton (1643-1727), Daniel Bernoulli (1700-1782), Leonhard Paul Euler (1707-1783), Jean le Rond D'Alembert (1717-1783), Joseph-Louis Lagrange (1736-1813), Pierre-Simon Laplace (1749-1827), Simeon-Denis Poisson (1781-1840) who later made further advancements in the field of continuum mechanics.

Torricelli is noted for the invention of the barometer and his works in static mechanics; Pascal for his clarification of the concepts of pressure and vacuum through his generalization of the work of Torricelli; Newton for his studies on viscous fluids and the concept of viscosity; Bernoulli for his extensive work in continuum mechanics in general and his introduction of mathematical fluid dynamics in his publication *Hydrodynamica* (1738); Euler for his studies on inviscid flow among many other achievements in the area of fluid mechanics; D'Alembert for

his Lagrange-D'Alembert (or simply D'Alembert) principle which is a statement of newtonian laws of motion; Lagrange for analysis of inviscid fluids and Lagrangian mechanics which is a reformulation of classical/Newtonian mechanics for ease of calculation through the combination of momentum and conservation of energy; Laplace for his analysis of inviscid fluids and his translation of Newton's work into the language of differential calculus in his five volume publication *Mecanique celeste (Celestial Mechanics)* and Poisson for his analysis of inviscid fluids, potential theory and correction of Laplace's second order partial differential equation to include potential.

3.1 Fluid Dynamics

3.1.1 Euler's Equations

Euler's equations were one of the first differential equations to be written down. They govern inviscid flow without heat conduction. Though the Energy balance (or adiabatic condition) was later added by Laplace in 1816, these equations are attributed to Euler. They are a set of transport equations for mass, momentum and energy in a closed system.

$$\frac{\partial \rho}{\partial t} + \nabla \cdot (\rho \overline{v}) = 0 \tag{3.2}$$

$$\frac{\partial \rho \overline{v}}{\partial t} + \nabla \cdot (\overline{v} \otimes (\rho \overline{v})) + \nabla P = 0 \tag{3.3}$$

$$\frac{\partial E}{\partial t} + \nabla \cdot (\overline{v}(E + P)) = 0 \tag{3.4}$$

where:
ρ is the fluid mass density,
$\overline{v}$ is the fluid velocity vector, with components u, v, and w,
P is the pressure.
E is the total energy per unit volume,
E = ρ e + $\frac{1}{2}$ ρ $(u^2 + v^2 + w^2)$, and
e is the internal energy per unit mass

Further developments leading to what we know today as fluid dynamics came from French European scientists Claude-Louis Navier (1785−1836) and George Gabriel Stokes (1819−1903) to whom the Navier-Stokes equation is named after.

3.1.2 Navier-Stokes Equation

The starting point in formulating most mathematical models involving fluid flow today is the Navier-Stokes equation. It is the general transport equation in its application to fluid dynamics. The equation comes from a differential calculus representation of Newton's second law to fluid motion, together with the assumption that the fluid stress, due to conduit wall friction, is the

sum of a diffusing viscous term proportional to the gradient of velocity, plus a pressure term. The Navier-Stokes equation coupled with other equations can also be used in a myriad of other applications other than fluid dynamics.

$$\rho\left(\frac{\partial \mathbf{v}}{\partial t} + \mathbf{v}\cdot\nabla\mathbf{v}\right) = -\nabla P + \nabla\cdot\mathbb{T} + \mathbf{f} \tag{3.5}$$

Where:
$\mathbf{v}$ is the flow velocity,
ρ is the fluid density,
P is the pressure,
$\mathbb{T}$ is the stress tensor, and
$\mathbf{f}$ represents body forces (per unit volume) acting on the fluid.

The Navier-Stocks equation is simply a statement of momentum conservation and in order to adequately describe the flow of fluids more information is needed.

3.2 The Governing Equations

Transient modeling of compressible flow is not an easy task due to the difficulty involved in obtaining the solution of the PDE describing the problem. In order to acquire preliminary understanding of the purpose for which we are doing the mathematics, we will like to keep the mathematics as simple as possible while maintaining a satisfactory level of practicality. This simplification comes in the form of the following assumptions:

1) Single phase Flow: The fluid maintains one continuous phase
2) Isothermal Flow: Temperature changes are negligible
3) Annular Flow: The flow is 1-D and remains annular such that any blockage in the pipe occurs symmetrically around the pipe

As mentioned earlier in section 3.1.2, the flow of fluids is not adequately described by the Navier-Stokes equation hence the need for additional information. Irrespective of assumptions, in order to adequately describe fluid flow, one must couple the mass balance equation to a Momentum balance equation. This is the simplest practical form of the mathematical description of fluid flow. However, a consideration of viscous effects will improve the formulation (Zhou and Adewumi, 1995a, 1995b; Ibrahim and Adewumi, 1996a, 1996b).

Taking the set of assumptions above into consideration, a one-dimensional representation of a single phase, isothermal, quasi-compositional natural gas model in a variable area pipe is given by:

$$\frac{\partial(\rho A)}{\partial t} + \frac{\partial(\rho A v)}{\partial x} = 0 \tag{3.6}$$

$$\frac{\partial(\rho A v)}{\partial t} + \frac{\partial((\rho v^2 + P)A)}{\partial x} = P\frac{\partial(A)}{\partial x} - F_f - F_g \tag{3.7}$$

where:
F_f = Friction force at the pipe wall, $\frac{lb_f}{ft^3}$
F_g = Gravitational force, $\frac{lb_f}{ft^3}$

The above equations can be unified into the one-dimensional, first-order, non-linear, non-homogeneous, hyperbolic PDE form below:

$$\frac{\partial \overrightarrow{Q}}{\partial t} + \frac{\partial(\overrightarrow{F}(\overrightarrow{Q}))}{\partial x} = \overrightarrow{G}(\overrightarrow{Q}) \tag{3.8}$$

where:

$$\overrightarrow{Q} = \begin{bmatrix} \rho A \\ \rho v A \end{bmatrix} \tag{3.9}$$

$$\overrightarrow{F}(\overrightarrow{Q}) = \begin{bmatrix} \rho v A \\ (\rho v^2 + P)A \end{bmatrix} \tag{3.10}$$

$$\overrightarrow{G}(\overrightarrow{Q}) = \begin{bmatrix} 0 \\ P\frac{\partial A}{\partial x} - F_f - F_g \end{bmatrix} \tag{3.11}$$

One of the advantages of this formulation is that the third assumption helps us avoid the need to impose boundary conditions at locations within the pipe where the inner diameter changes. However, this implies that the roughness of the wall of the pipe is assumed to be correspondent to that of the blockage material.

Furthermore, in order to have a well defined problem we must have the same number of equations as unknowns, but the two equations above features three unknown variables (density, Velocity and Pressure). To resolve this problem, we know that density can easily be defined as a function of pressure through equations of states (EOSs), hence a third equation. This equation is a simple isothermal EOS which includes the gas compressibility factor (z) and this will aid us in incorporating the effect of real gases on the system.

$$P = \frac{zRT}{M_g}\rho \tag{3.12}$$

where:

z = gas compressibility factor
R = Universal Gas Constant (10.731 $\frac{psift^3}{lbmolR}$)
T = Isothermal Temperature (R)
M_g = Molecular Weight (lbm/lbmol)

Given the pressure profile and temperature within the pipe, the acoustic wave speed within the pipe can also be determined by:

$$c = (\frac{Pg_c}{\rho})^{\frac{1}{2}} = (\frac{zRT}{M_g})^{\frac{1}{2}} \tag{3.13}$$

3.3 The constitutive Equations

3.3.1 The Frictional Force

The frictional force is a shear force that represents the inertia term in the Navier-Stokes equation. It retards the flow of fluids within the pipe. In the formulation above, its effect is assumed to be distributed evenly around the cylindrical pipe surface and it is calculated as a function of friction factor (f):

$$F_f = \frac{2f\rho|v|v}{dg_c} \tag{3.14}$$

For laminar flow the fanning friction factor is:

$$f = \frac{16}{N_{Re}} \tag{3.15}$$

For turbulent flow we use Chen's Equation (1979):

$$\frac{1}{\sqrt{f}} = -4log\{\frac{(\frac{\varepsilon}{d})}{3.7065} - \frac{5.0452}{N_{Re}}log[\frac{(\frac{\varepsilon}{d})^{1.1098}}{2.8257} + \frac{5.8506}{N_{Re}^{0.8981}}]\} \tag{3.16}$$

where:
ε is pipe roughness d is pipe diameter N_{Re} is the Reynolds number

$$N_{Re} = \frac{\rho vd}{\mu} \tag{3.17}$$

3.3.2 The Gravitational Force

This term allows for the simulation of the effects of pipe inclination with respect to the horizontal axis. For a horizontal pipe, this term drops out of the formulation because it is then equal to zero as can be inferred from the equation below.

$$\frac{F_g = \rho g \sin\theta}{g_c} \tag{3.18}$$

3.4 Fluid Properties

3.4.1 Gas Viscosity

Gas viscosity is estimated using Lee, Gonzalez and Eakin (1966) correlation given below:

$$\mu = Kexp(X(\frac{\rho}{62.4})^y) \tag{3.19}$$

where:
K = $T^{1.5}$ $\frac{(9.4+0.02M_g)}{10^4(209+19M_g+T)}$
X = 3.5 + 0.01M_g - $\frac{986}{T}$
y = 2.4-0.2X

Fluid viscosities estimated using the above equation are in good agreement with measured values and have a standard deviation of ±2.7 percent for a temperature range of 100 to 340 degree Fahrenheit and a pressure range of 100 to 8000 psia.

3.4.2 Gas Compressibility

The Peng-Robin equation of state is used to estimate the gas compressibility at new time step in this formulation. See Appendix for more detail.

Chapter 4

The Numerical Technique

4.1 Finite Volume Method

Finite volume method (FVM) is based upon subdividing the spatial domain into sections also known as finite volumes (or grid cells) and then keeping track of the approximations to the integral of continuous function(s) over each section/segment. FVMs are closely related to finite difference methods (FDMs) and a FVM can be interpreted as a direct finite difference approximation to differential equations without separation of variables by chain rule. Unlike the FDM, the FVM is derived on the basis of the integral form of the conservation laws thereby mimicking the true solution and ensuring that the numerical method is conservative. The conservative property of the FVM is extremely important for shock wave modeling and this is because the summation of the piecewise approximations of each finite volume (or grid cell) over the entire section (or interval) approximates the integral of the continuous function such that the discrete sum will change only due to fluxes at the boundary. Therefore, when applied to the mass conservation equation, the total mass within the domain (or system) is preserved or will vary appropriately at the boundaries.

4.1.1 Piecewise Constant Averages for Grid Cells

$$\frac{\partial q}{\partial t} + \frac{\partial (f(q))}{\partial x} = 0 \tag{4.1}$$

Consider the hyperbolic PDE as described above where $q = q(x, t_n)$ is a smooth continuous function. If we denote the i^{th} grid cell as $S_i = (x_{i-\frac{1}{2}}, x_{i+\frac{1}{2}})$. The value Q_i^n will represent the approximated average of the continuous function, q, over the i^{th} interval at time t_n:

$$Q_i^n \cong \frac{1}{\Delta x} \int_{x_{i-\frac{1}{2}}}^{x_{i+\frac{1}{2}}} q(x, t_n) dx \equiv \frac{1}{\Delta x} \int_{S_i} q(x, t_n) dx \tag{4.2}$$

where $\Delta x = x_{i+\frac{1}{2}} - x_{i-\frac{1}{2}}$, is the length of a cell. For simplicity we will be using uniform grid sizes through out this work.

4.1.2 The Integral Form of the Conservation Laws

As mentioned earlier FVM involves discretizing the system such that each piecewise constant estimate approximates the integral of the continuous function (q) over an interval. Consider the equation 4.1 above. If we integrate equation 4.1 across a finite volume (or grid cell) denoted S_i we will obtain the following:

$$\frac{d}{dt}\int_{S_i} q(x,t)dx + \frac{d}{dx}\int_{S_i} f(q(x,t))dx = 0 \tag{4.3}$$

Or better still, the above equation can be rewritten as:

$$\frac{d}{dt}\int_{S_i} q(x,t)dx + (f(q(x_{i+\frac{1}{2}},t)) - f(q(x_{i-\frac{1}{2}},t))) = 0 \tag{4.4}$$

Integrating equation 4.4 in time within the time interval, t_n and t_{n+1} gives:

$$\begin{aligned}&\left(\int_{S_i} q(x,t_{n+1})dx - \int_{S_i} q(x,t_n)dx\right) + ... \\ &\left(\int_{t_n}^{t_{n+1}} f(q(x_{i+\frac{1}{2}},t))dt - \int_{t_n}^{t_{n+1}} f(q(x_{i-\frac{1}{2}},t))dt\right) = 0\end{aligned} \tag{4.5}$$

We can then obtain the piece wise averages to each grid cell as defined in equation 2.2 simply by dividing through equation 4.5 by Δx.

$$\begin{aligned}&\left(\frac{1}{\Delta x}\int_{S_i} q(x,t_{n+1})dx - \frac{1}{\Delta x}\int_{S_i} q(x,t_n)dx\right) + ... \\ &\frac{1}{\Delta x}\left(\int_{t_n}^{t_{n+1}} f(q(x_{i+\frac{1}{2}},t))dt - \int_{t_n}^{t_{n+1}} f(q(x_{i-\frac{1}{2}},t))dt\right) = 0\end{aligned} \tag{4.6}$$

Or better still:

$$(Q_i^{n+1} - Q_i^n) + \frac{1}{\Delta x}\left(\int_{t_n}^{t_{n+1}} f(q(x_{i+\frac{1}{2}},t))dt - \int_{t_n}^{t_{n+1}} f(q(x_{i-\frac{1}{2}},t))dt\right) = 0 \tag{4.7}$$

This tells us exactly how the average value of the continuous function(q) should be updated in one time step. Note that we have not made any approximations so far and the above equation is still exact assuming that the piece wise constant averages are properly evaluated. However, time

integral of the flux terms in equation 4.7 above can not evaluated exactly because the continuous function (q) varies along both edges of the grid cell. Hence we approximate the average time integral of the flux terms as $F^n_{i\pm\frac{1}{2}}$. Therefore, rewriting equation 4.7 gives:

$$(Q_i^{n+1} - Q_i^n) + \frac{\Delta t}{\Delta x}\left(F^n_{i+\frac{1}{2}} - F^n_{i-\frac{1}{2}}\right) = 0 \tag{4.8}$$

Where:

$F^n_{i+\frac{1}{2}}$ = the average time integral of the flux term at the right edge of the grid cell, S_i at time t_n. Also known as the numerical flux function.

$$F^n_{i+\frac{1}{2}} \approx \frac{1}{\Delta t}\int_{t_n}^{t_{n+1}} f(q(x_{i+\frac{1}{2}}, t))dt \tag{4.9}$$

The method used to evaluate the average time integral of the flux term is determined by the numerical scheme adopted. Numerical schemes will be discussed later.

4.1.3 The Conservative Nature of FVM

Equation 4.8 is said to be in the conservative form since it mimics the exact form (Equation 4.6). If we were to sum $\Delta x Q_i^{n+1}$ from equation 4.4 over any set of cells we obtain:

$$\Delta x \sum_{i=I}^{J} Q_i^{n+1} = \Delta x \sum_{i=I}^{J} Q_i^n - \frac{\Delta t}{\Delta x}\left(F^n_{J+\frac{1}{2}} - F^n_{I-\frac{1}{2}}\right) \tag{4.10}$$

It is therefore clear that with the exception of the boundaries (extreme ends of the full domain) in the system , the sum of flux differences cancel out. As a result we have exact conservation over the full domain except at the boundaries.

4.1.4 FVM or Direct Finite Difference of the Conservation Laws

The finite volume method can be viewed as a direct finite difference approximation of equation 4.1. Just for pedagogical reasons, if we divide equation 4.8 by Δt, we obtain:

$$\frac{(Q_i^{n+1} - Q_i^n)}{\Delta t} + \frac{(F^n_{i+\frac{1}{2}} - F^n_{i-\frac{1}{2}})}{\Delta x} = 0 \tag{4.11}$$

However, what makes finite volume a conservative method is the fact that Q_i^n are piece wise averages for each grid cell and $F^n_{i\pm\frac{1}{2}}$ are the average time integrals of the whole flux term at the left and right edges of the grid cell, S_i at time, t_n. Finite difference method instead uses linear approximations in the form of finite slopes to approximate the continuous function. This is what makes the FDM unsuitable for non-linear functions especially when dealing with sharp fronts like

expect when solving non-linear hyperbolic PDEs. However, FDM is quite sufficient for modeling linear or smoother functions.

4.2 Convergence requirements

Before discussing the various numerical schemes that can be used to approximate the flux functions it is important to highlight some important requirements for convergence while using any finite volume numerical scheme. One important requirement is that the numerical scheme must be convergent. Meaning that as grid is refined (i.e. Δt and $\Delta x \rightarrow 0$), the solution should converge to the real integral form discussed earlier. For a numerical scheme to be convergent, it must satisfy two conditions:

1. Numerical Consistency: This means that the numerical scheme adopted must approximate the flux function very well using the adjacent blocks.

2. Stability: Stability requirements vary from problem to problem. However, regardless of the type of problem being solved (whether linear or non-linear, hyperbolic or parabolic etc.), a numerical scheme must satisfy the Courant-Friedrichs-Lewy (CFL) conditions. Secondly, the error that arises as one marches along the time domain must not grow too fast.

4.2.1 Numerical Consistency

As mentioned briefly above, consistency in a numerical scheme implies that the scheme approximates the flux functions satisfactorily. This means that if the average block estimates of the continuous function (q(x,t)) of two blocks at one edge for which we are estimating the flux function is equal to $\overline{q}$, then the approximated flux function, $\mathbf{F}(Q_i, Q_{i\pm1})$, at that edge between Q_i and $Q_{i\pm1}$ must be equal to f($\overline{q}$).

i.e., If

$$Q_i = Q_{i+1} = \overline{q} \tag{4.12}$$

then

$$F_{i+1}(Q_i, Q_{i+1}) = f(\overline{q})) \tag{4.13}$$

4.2.2 Stability

For any FVM or FDM the CFL condition is necessary for convergence though as already mentioned briefly, satisfying the CFL condition does not guarantee stability. The CFL condition states that *"a numerical method can be convergent only if its numerical domain of dependence contains the true domain of dependence of the PDE [being approximated], at least in the limit as Δt and $\Delta x \rightarrow 0$"* (LeVeque, 2002)[18].

In simpler terms, the average piecewise constant approximation of the continuous function, (q(x,t)), at the grid cell "S_i" and new time step, t_{n+1}, (i.e. Q_i^{n+1}), is a function of some average piecewise constant estimates around and possibly including the i^{th} grid cell from the previous time step, t_n. Therefore, for the CFL condition to be satisfied, the approximate value, Q_i^{n+1} must be determined as a function of the appropriate average piecewise constant estimates, Q_I^n. where I includes all blocks at time, t_n for which Q_i^{n+1} is dependent on. Figure 4.1 illustrates this point. For a centered three-point stencil numerical scheme, the time step size must not be larger than $\Delta t = t'_{n+1} - t_n$ (see Figure 4.1). Note that if the time step is small enough, the information needed to determine Q_i^{n+1} can be obtained from the adjacent blocks (Q_{i-1}^n, Q_i^n, Q_{i-1}) only. This is especially very important if we choose to utilize a centered three-point stencil numerical scheme.

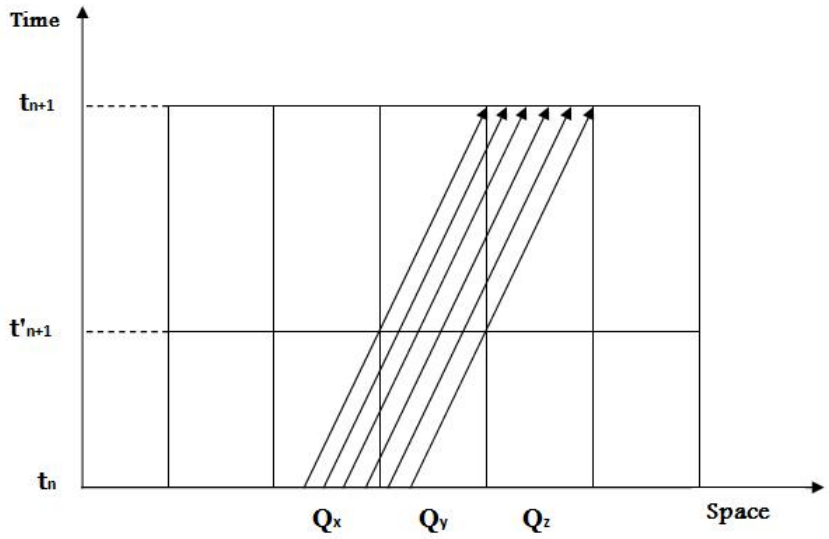

Figure 4.1: Domain of Dependence

The question now becomes: "So how can I ensure that my numerical domain of dependence contains the true domain of dependence of the PDE?" or better still, "If I already know the stencil size I will be using based on the numerical scheme I choose, how can I ensure that I keep the time step small enough such that the true domain of dependence of my PDE is within the stencil range I am using ?"

4.2.2.1 Courant Number

The answer to the question above is the courant number (ν) also known as the CFL number (R. Courant K. Friedrichs and H. Lewy, 1967). For a closed linear PDE (or conservation equation)

of the form in equation 4.14 below, the courant number is a function of the constant wave speed ($\overline{v}$).

$$\frac{\partial q}{\partial t} + \overline{v}\frac{\partial (q)}{\partial x} = 0 \tag{4.14}$$

For the linear PDE 4.14 above The courant number can be determined using the following equation:

$$\nu \equiv \left| \overline{v}\frac{\Delta t}{\Delta x} \right| \leq 1 \tag{4.15}$$

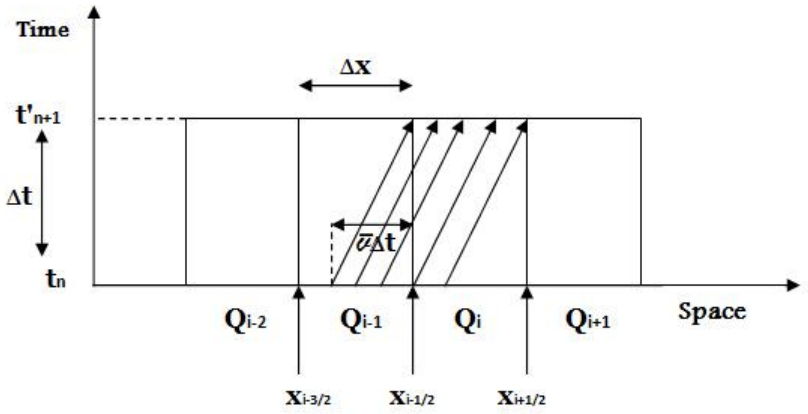

Figure 4.2: Upwind Linear Extrapolation

Using a centered three-stencil scheme to approximate the linear flux term in equation 4.14, the CFL condition can only be satisfied if courant number is less than or at most equal to 1. Visually, one can observe from Figure 4.2 that if Q_i^{n+1} is to be approximated as a simple extrapolation from time step n to n+1 to obtain equation 4.16 below, $\overline{v} \times \Delta t$ must be greater than Δx or else, the true domain of dependence will no longer be within the range of a centered three-stencil numerical scheme.

$$Q_i^{n+1} = Q_i^n - \frac{Q_i^n - Q_{i-1}^n}{\Delta x}\left[x_{i-\frac{1}{2}} - (x_{i-\frac{1}{2}} - \overline{v}\Delta t)\right] \tag{4.16}$$

For a system of PDE's, the courant number is a function of the maximum wave speed. And in case of a non-linear set of PDE's (or conservation equations) of the form in equation 4.1 which we are concerned about, the courant number is a function of the maximum eigen value from the Jacobian matrix obtained from the flux terms as a function of the vector $\overrightarrow{Q}$.

$$\nu \equiv max(|\lambda|) \times \frac{\Delta t}{\Delta x} \leq 1 \tag{4.17}$$

4.2.3 Additional Stability requirements for Non-linear PDEs

As mentioned earlier the CFL condition is a requirement for stability of a numerical scheme but not sufficient to ensure stability. Depending on the kind PDE being solved there may exist additional requirements. Here we will focus on non-linear conservation laws since that is what we are trying to solve.

4.2.3.1 Monotone Property

For non-linear scalar conservation laws, the use of a numerical scheme with monotone property in addition to satisfying the CFL condition is sufficient for stability since the monotone property implies that such a scheme is contractive in some norm (LeVeque, 2002). For a numerical scheme to possess the monotone property, an increase in the approximated variable, Q_I^n (where I represents any grid cell "i" in the full domain) at time step n must follow an increase in the approximated variable, Q_J^{n+1} (where J represents any grid cell "j" in the full domain) at time step t_{n+1} and vice-versa. i.e. a numerical scheme has the monotone property if:

$$\frac{\delta Q_I^{n+1}}{\delta Q_J^n} \geq 0 \tag{4.18}$$

4.2.3.2 TVD and TVB Property

For non-linear numerical schemes (or methods) such as higher resolution methods involving the use of limiters that are themselves dependent on the original data, a stronger contractive property is required for stability. Numerical methods with the Total Variation Non-increasing (TVNI) (or Total Variation Diminishing (TVD)) property are effective tools for ensuring stability of non-linear problems. A numerical method is Total Variation Bounded (TVB) if:

$$TV(Q^n) \leq R \tag{4.19}$$

For any time, nΔt < T whenever $\Delta t < \Delta t_0$
where:

$$\begin{aligned} T &= n_{max}\Delta t \\ R &= AConstantValue \\ \Delta t_0 &= \Delta t \ @ \ Q^0 \end{aligned}$$

This means that for any data Q^0, and time, T, there is a constant R and a value $\Delta t_0 > 0$ such that the total variation for any data Q^n is less than or equal to R. A numerical method with TVD property has the TVB property with TV(Q^n) = R.

4.3 Numerical Schemes

In order to have a fully discretized system, the average time integral of the flux term (or the numerical flux) at each edge of the cell block of interest, "S_i", in equation 4.8 must be approximated using an appropriate numerical scheme. This approximation should be done such that Q_i^{n+1} is a function dependent on the surrounding cell blocks of S_i. That is:

For a centered three-point stencil explicit scheme:

$$F_{i+\frac{1}{2}}^n = \mathbf{F}(Q_i^n, Q_{i+1}^n) \tag{4.20}$$

Therefore equation 4.8 becomes:

$$(Q_i^{n+1} - Q_i^n) + \frac{\Delta t}{\Delta x}\left(\mathbf{F}(Q_i^n, Q_{i+1}^n) - \mathbf{F}(Q_{i-1}^n, Q_i^n)\right) = 0 \tag{4.21}$$

In this section, we will be discussing the various numerical schemes studied for a hyperbolic system of the form in Eq. 4.1.

4.3.1 Lax-Friedrichs Method

For a three-point stencil scheme, where the flux functions at both edges of the block S_i are to be estimated as a function of Q_{i-1}, Q_i, Q_{i+1}, one might want use a simple arithmetic average of the Q-values at the grid blocks left and right of an edge as follows:

$$F_{i+\frac{1}{2}}^n = \mathbf{F}(Q_i^n, Q_{i+1}^n) = \frac{1}{2}[f(Q_i^n) + f(Q_{i+1}^n)] \tag{4.22}$$

so that equation 4.21 becomes:

$$(Q_i^{n+1} - Q_i^n) + \frac{\Delta t}{\Delta x}\left(\frac{1}{2}[f(Q_i^n) + f(Q_{i+1}^n)] - \frac{1}{2}[f(Q_{i-1}^n) + f(Q_i^n)]\right) = 0 \tag{4.23}$$

after some arithmetic manipulation the equation above becomes:

$$(Q_i^{n+1} - Q_i^n) + \frac{\Delta t}{2\Delta x}(f(Q_{i+1}^n) - f(Q_{i-1}^n)) = 0 \tag{4.24}$$

However, there is a problem. The equation above happens to be unstable for hyperbolic PDEs, so we can not use it to solve our problem. In order to make the equation above stable Peter Lax and Kurt O. Friedrichs introduced an artificial viscosity term to the numerical flux so that it takes the form:

$$F^n_{i+\frac{1}{2}} = \frac{1}{2}[f(Q^n_i) + f(Q^n_{i+1})] - \lambda'(Q^n_{i+1} - Q^n_i) \tag{4.25}$$

where:

$$\lambda' = \frac{\Delta x}{\Delta t} \tag{4.26}$$

Replacing the numerical flux terms with that of Lax-Friedrichs and applying some arithmetic manipulations, Equation 4.21 then becomes:

$$\left[Q^{n+1}_i - \frac{1}{2}(Q^n_{i-1} + Q^n_{i+1})\right] + \frac{\Delta t}{2\Delta x}(f(Q^n_{i+1}) - f(Q^n_{i-1})) = 0 \tag{4.27}$$

The formulation above is known as the Lax-Friedrichs method. There are other variations of this numerical scheme depending on the definition of λ. This numerical scheme is generally stable and gives reasonable results. However, for our problem the accuracy of the results dissipates over time and the spacial resolution is very poor for shock wave problems. It also tends to provide solutions that are not as smooth if care is not taken with the solver adopted. Another important point to mention, though not observed in our numerical experiment is that Lax-Friedrichs numerical method typically produces results that are badly smeared unless very fine grid is used.

4.3.2 The Richtmyer Method

The Richtmyer method also known as the Two-Step Lax-Wendroff Method for non-linear PDE's is a modification of the Lax-Wendroff Method used for linear PDE's. This provides second order accuracy in time simply by approximating q at half time step, $t_{n\pm\frac{1}{2}}$ using the Lax-Friedrichs (L-F) scheme as in equation 4.29 prior to evaluating the numerical flux functions using the mid-time step approximation. The Richtmyer method evaluation of the numerical flux function is as follows:

$$F^n_{i+\frac{1}{2}} = f(Q^{n+\frac{1}{2}}_{i+\frac{1}{2}}) \tag{4.28}$$

where:

$$Q_{i+\frac{1}{2}}^{n+\frac{1}{2}} = \frac{1}{2}(Q_{i-1}^{n} + Q_{i+1}^{n}) - \frac{\Delta t}{2\Delta x}(f(Q_{i+1}^{n}) - f(Q_{i}^{n})) \tag{4.29}$$

This methods provides the same spacial resolution as does the L-F scheme. However, the accuracy of the solution over time does not dissipate as fast thereby giving this method an advantage over the L-F method though it is a little bit more computationally involved.

The numerical schemes mentioned so far are best used when one has no idea of the directions of wave propagation in the system. However, with the knowledge of the direction of disassembled waves propagation in a system of equations, can help us determine a better approximation the numerical flux term that will yield better spacial resolution with out necessarily increasing computational load.

4.3.3 The First-Order Upwind Method

The knowledge of the direction of disassembled waves moving along characteristics in hyperbolic conservation laws helps in identifying the domain of dependence of Q_i^{n+1}. So therefore, for an advection equation such as the mass balance equation, given a small enough time step size and assuming that the positive direction of flow is from left to right, the flux through the left and right edges of a grid cell "S_i" can be entirely dependent on Q_{i-1} and Q_i respectively.

This implies that we can define the flux at the right and left edges of the grid cell "S_i" as:

$$F_{i+\frac{1}{2}}^{n} = \mathbf{F}(Q_i^n) \quad \& \quad F_{i-\frac{1}{2}}^{n} = \mathbf{F}(Q_{i-1}^n) \tag{4.30}$$

Applying equation 4.30 above to equation 4.8 leads to a first order version of the standard Upwind method of the form:

$$(Q_i^{n+1} - Q_i^n) + \frac{\Delta t}{\Delta x}(f(Q_i^n) - f(Q_{i-1}^n)) = 0 \tag{4.31}$$

As can be inferred from equation 4.31 above, the First-order Upwind method is less computationally involved and yet provides better spacial resolution which is very important in modeling shock waves.

It is important to note that this first-order upwind scheme is essentially a linear extrapolation from one time step to another. This can be illustrated by a little algebraic manipulation of equation 4.16 which is simply a linear extrapolation as was discussed earlier. This will yield the upwind scheme for a linear hyperbolic PDE as shown in equation 4.32 below:

$$(Q_i^{n+1} - Q_i^n) + \overline{v}\frac{\Delta t}{\Delta x}(Q_i^n - Q_{i-1}^n) = 0 \tag{4.32}$$

Equation 4.31 forms the basis for the final form of the numerical scheme applied in this work. However, to accommodate the physics of actual problem a slight twist is applied to the two-point stencil upwind scheme above to convert it to a three-point stencil upwind scheme as will be discussed section 4.4. It is important to note that first-order upwind methods have the advantage of keeping the solution monotonically varying in regions where the solution should be monotone (LeVeque, 2002).

4.3.4 Nessyahu and Tadmor centered scheme

So far we have considered only first-order schemes. In order to obtain higher order accuracy in space we can redefine the way we approximate the numerical flux function for second-order accuracy. This is achieved by the use of piecewise linear approximations of the continuous function as opposed to piecewise constant approximations used in previously discussed schemes. Although there are simpler methods for reconstructing the data (Q_i^n) for second order accuracy such as a simple linear extrapolation, these methods like most second order accurate schemes, are known to produce spurious oscillations at discontinuities and do not have the TVD property. However, Van Leer (1979) proposed a slope limited linear reconstruction technique known as the MUSCL (Monotone Upstream-centered Schemes for Conservation Laws) reconstruction. This is the first high-order TVD reconstruction technique ever proposed.

MUSCL reconstruction is relatively easy to implement and will also be considered in this work. If we reconstruct the data (Q_i^n) by an extrapolation to obtain both the left and right states at both edges of each cell (see figure 4.3) as described in equation 4.33 to 4.36 we can define the numerical flux function as $\mathbf{F}(Q^L_{i\pm\frac{1}{2}}, Q^R_{i\pm\frac{1}{2}})$.

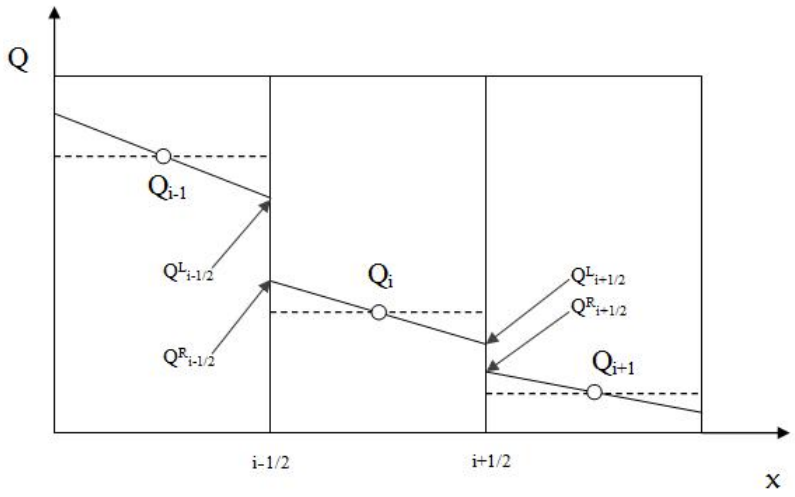

Figure 4.3: Linear Reconstruction

$$Q^L_{i+\frac{1}{2}} = Q_i + 0.5\phi\left(r_i\right)\left(Q_{i+1} - Q_i\right) \tag{4.33}$$

$$Q^R_{i+\frac{1}{2}} = Q_{i+1} - 0.5\phi\left(r_{i+1}\right)\left(Q_{i+2} - Q_{i+1}\right) \tag{4.34}$$

$$Q^L_{i-\frac{1}{2}} = Q_{i-1} + 0.5\phi\left(r_{i-1}\right)\left(Q_i - Q_{i-1}\right) \tag{4.35}$$

$$Q^R_{i-\frac{1}{2}} = Q_i - 0.5\phi\left(r_i\right)\left(Q_{i+1} - Q_i\right) \tag{4.36}$$

where:
$\phi(r)$ is a slope limiter
r is the measure of smoothness of the data around an edge and defined as: $r_i = \frac{Q_i - Q_{i-1}}{Q_{i+1} - Q_i}$

Once we have the reconstructed left and right states at the edges of each grid cell, we may now apply it to any numerical scheme where the numerical flux function can be defined as $\mathbf{F}(Q^L_{i\pm\frac{1}{2}}, Q^R_{i\pm\frac{1}{2}})$. However, in order to obtain these values we still need a limiter. There are many limiters in the literature but we will be using the Monotonized Central (MC) limiter which is a symmetric limiter also proposed by Van Leer (1977). The MC limiter is well noted as a good default choice for a wide range of problems (LeVeque, 2002) and is defined as follows:

$$\phi_{mc}(r) = \max[0, \min(2r, 0.5(1+r), 2)] \tag{4.37}$$

where:
$\lim_{r\to\infty} \phi_{mc}(\mathrm{r}) = 2$ We can now introduce a numerical schemes that allows the definition of

the numerical flux function as $\mathbf{F}(Q^L_{i\pm\frac{1}{2}}, Q^R_{i\pm\frac{1}{2}})$. As a modification to the Lax-Friedrichs centered scheme, Nessyahu and Tadmor (1990) proposed the following NT centered scheme that utilizes linear reconstruction:

$$F^n_{i+\frac{1}{2}} = \frac{1}{2}[f(Q^L_{i+\frac{1}{2}}) + f(Q^R_{i+\frac{1}{2}})] - \lambda'(Q^R_{i+\frac{1}{2}} - Q^L_{i+\frac{1}{2}}) \tag{4.38}$$

where:
$\lambda' = \frac{\Delta x}{\Delta t}$

4.4 One-Dimensional Symmetrical Griding Systems

Two single-dimensional symmetrical finite volume griding options are discussed for allegorical reasons.

4.4.1 Regular/Collocated Finite Volume (FV) Grid

The application of the finite volume method (FVM) implies that we are estimating grid cell averages of the continuous function q. From our mathematical formulation we know that q is a vector of two variables, density and mass flux. Density which is related to pressure is a scalar quantity while mass flow rate which is related to velocity is a vector quantity. Using the regular FV grid both density and mass flow rate are estimated at the same location as illustrated in the Figure below.

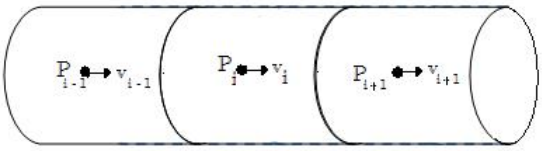

Figure 4.4: Collocated Grid

For the problem we are trying solve, this griding system is known to produce spurious pressure results at wave fronts or discontinuities. However, this griding system is used for all the centered schemes discussed in section 4.3.

4.4.2 Staggered Grid Approach

Here the vector variables are estimated at the edges of the grid cell S_i, while the scalar variables are estimated at the center as illustrated below. It is known as the half-staggered griding system. For the system of hyperbolic PDEs we are concerned about, this grid system is ideal and well tested with FVM (C.Frepoli, et al., 2000 and 2003). It is also broadly used with FDM.

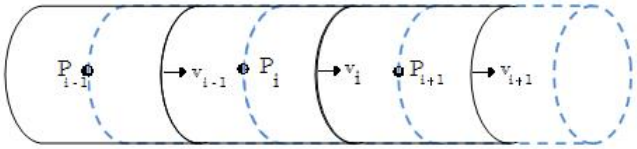

Figure 4.5: Staggered Grid

This gridding system will be employed in the two-point stencil upwind numerical approximation of our system of equations thereby transforming it into a three-point stencil upwind

scheme.

4.5 Treatment of Source Terms

So far we have treated the source term like it did not exist through out our formulations. However, like we discussed in chapter 3, inclusion of the source terms in the momentum equation will help to improve the physical practicality of our mathematical model.

4.5.1 The Half Step Method

One approach is to use a half step model where we solve the simpler homogeneous problem of the form in equation 4.8 and then we are left with an ODE of the form below which is then solved using various ODE solvers. This method is widely used but is a bit more computationally demanding.

$$\frac{d(\overrightarrow{Q})}{dt} = \overrightarrow{G}(\overrightarrow{Q}) \tag{4.39}$$

where:
$\overrightarrow{G}(\overrightarrow{Q})$ is a vector of the non-linear source terms from the system of equations.

4.5.2 The Unsplit Method

Another approach is the Unsplit method which more clearly models the correct equation (LeVeque, 2002). Here the source term is simply included in the equation so that equation 4.8 becomes:

$$(Q_i^{n+1} - Q_i^n) + \frac{\Delta t}{\Delta x}\left(F^n_{i+\frac{1}{2}} - F^n_{i-\frac{1}{2}}\right) = G(Q_i) \tag{4.40}$$

This approach will be applied in our numerical discretization due to its simplicity. For the centered schemes, average values are obtained at the edges of the blocks where necessary.

4.6 The Fully Discretized System of Equations

A fully discretized explicit form of our mathematical model using the unsplit staggered three point stencil upwind scheme yields the following algebraic equations:

Mass Conservation Equation {units: lbm/ft} :

$$[(\rho_i A_i)^{n+1} - (\rho_i A_i)^n] + \lambda\left[(\rho_i v_i A_i)^n - (\rho_{i-1} v_{i-1} A_{i-1})^n\right] = 0 \tag{4.41}$$

Momentum Conservation Equation {units: lbm/s} :

$$\begin{aligned}
&[(\rho_i v_i A_i)^{n+1} - (\rho_i v_i A_i)^n] + ... \\
&\lambda \left[(\rho_{i+1} v_{i+1}^2 A_{i+1} + 144 g_c P_{i+1} A_{i+1})^n - (\rho_i v_i^2 A_i + 144 g_c P_i A_i)^n\right] - ... \\
&\lambda 144 g_c P_i^n (A_{i+1} - A_i) + \Delta t F_f^n g_c A_i = 0
\end{aligned} \tag{4.42}$$

where:

$$\begin{aligned}
A &= \text{Pipe Area}, ft \\
v &= \text{Gas Velocity}, \frac{ft}{s} \\
P &= \text{Pressure}, \frac{lb_f}{in^2} \\
\rho &= \text{Gas Density}, \frac{lb_m}{ft^3} \\
g_c &= \text{standard gravity}, (32.174 \frac{ft}{s^2}) \\
144 &= \text{conversion factor for pressure from} \frac{lb_f}{in^2} to \frac{lb_f}{ft^2} \\
\lambda &= \frac{\Delta t}{\Delta x}
\end{aligned}$$

Note that the momentum equation is staggered downstream relative to the direction of flow. The fully implicit form is:

Mass Conservation Equation {units: lbm/ft} :

$$[(\rho_i A_i)^{n+1} - (\rho_i A_i)^n] + \lambda \left[(\rho_i v_i A_i)^{n+1} - (\rho_{i-1} v_{i-1} A_{i-1})^{n+1}\right] = 0 \tag{4.43}$$

Momentum Conservation Equation {units: lbm/s} :

$$\begin{aligned}
&[(\rho_i v_i A_i)^{n+1} - (\rho_i v_i A_i)^n] + ... \\
&\lambda \left[(\rho_{i+1} v_{i+1}^2 A_{i+1} + 144 g_c P_{i+1} A_{i+1})^{n+1} - (\rho_i v_i^2 A_i + 144 g_c P_i A_i)^{n+1}\right] - ... \\
&\lambda 144 g_c P_i^{n+1} (A_{i+1} - A_i) + \Delta t F_f^{n+1} g_c A_i = 0
\end{aligned} \tag{4.44}$$

4.7 Steady-State Solution

As can be inferred from our mathematical formulation, the time derivative of the hyperbolic PDE is equal to zero when the fluid is at steady state. So we are left with an ODE of spacial dependence. The mathematical formulation of the steady state solution is of the form:

Steady State Mass Conservation Equation

$$\frac{d(\rho A v)}{dx} = 0 \tag{4.45}$$

Steady State Momentum Conservation Equation

$$\frac{d((\rho v^2 + P)A)}{dx} = P\frac{d(A)}{dx} - F_f - F_g \tag{4.46}$$

where:
F_f = Friction force at the pipe wall, $\frac{lb_f}{ft^3}$
F_g = Gravitational force, $\frac{lb_f}{ft^3}$

The Fully discretized implicit version is of the form:

Mass Conservation Equation {units: lbm/s} :

$$(\rho_i v_i A_i)^{n+1} - (\rho_{i-1} v_{i-1} A_{i-1})^{n+1} = 0 \tag{4.47}$$

Momentum Conservation Equation {units: lbm-ft/s^2} :

$$\begin{aligned}&[(\rho_{i+1} v_{i+1}^2 A_{i+1} + 144 g_c P_{i+1} A_{i+1})^{n+1} - (\rho_i v_i^2 A_i + 144 g_c P_i A_i)^{n+1}]... \\ &- 144 g_c P_i^{n+1}(A_{i+1} - A_i) + F_f^{n+1} g_c \Delta x A_i = 0\end{aligned} \tag{4.48}$$

4.8 Numerical Solver: GNR

The Generalized Newton-Raphson (GNR) iterative technique was employed to simultaneously solve the fully-implicit version of the non-linear system of two algebraic equations in every grid block within the system. This means that we are simultaneously solving a set of equations equal to twice the number of blocks in the system to obtain the solution of unknown variables that are twice the number of blocks in the system. If the set of equations is written as:

$$\overrightarrow{F}(\overrightarrow{x}) = [f1(\overrightarrow{x}), f2(\overrightarrow{x}), ..., f_N(\overrightarrow{x})]^T = 0 \tag{4.49}$$

where:
$\overrightarrow{x}$ is the array of variables from every grid cell.

From a first order Taylor series expansion of $\overrightarrow{F}(\overrightarrow{x}^{m+1})$ about the approximate solution at the iteration level, m, i.e. $\overrightarrow{x}^m$ we have:

$$\overrightarrow{F}(\overrightarrow{x}^{m+1}) \approx \overrightarrow{F}(\overrightarrow{x}^{m}) + \frac{\partial \overrightarrow{F}}{\partial \overrightarrow{x}^{m}} \delta \overrightarrow{x}^{m} = \overrightarrow{F}(\overrightarrow{x}^{m}) + \overline{J}^{m} \delta \overrightarrow{x}^{m} \tag{4.50}$$

where $\overline{J}^{m}$ = Jacobian Matrix.

GNR is an iterative method that seeks the solution update $\delta \overrightarrow{x}^{m}$ that drives $\overrightarrow{F}(\overrightarrow{x}^{m+1})$ to zero. So if we set the left hand side of equation to zero, we are essentially solving the linear system of equations:

$$\overline{J}^{m} \delta \overrightarrow{x}^{m} = -\overrightarrow{F}(\overrightarrow{x}^{m}) \tag{4.51}$$

where:

$\overrightarrow{F}(\overrightarrow{x}^{m})$ is a vector of residuals calculated using variables from the previous iteration level, m.

The new solution at iteration level, m, is updated as follows:

$$\overrightarrow{x}^{m+1} = \overrightarrow{x}^{m} + \delta \overrightarrow{x}^{m} \tag{4.52}$$

This greatly reduced computational time while maintaining physical consistency of the model and ensuring better convergence due to the strict convergence criteria applied. Most runs converge in three iterations and computational speed is greatly determined by how finely defined is the grid system. All necessary adjustments necessary to make the GNR technique more efficient have been studied and well documented by C.Frepoli et al (2003).

4.9 Boundary Condition

The boundary condition applied have significant effect on the numerical solution especially considering the fact that finite volume method is a conservative method whereby variations in the conserved variables only occur at the boundaries. Since we have a system of two equations and two unknowns, there must be two boundary specifications both at bounds of the domain (i.e. pipe inlet and outlet).

One method for boundary specification is a first-order linear extrapolation from within the domain, also known as the zero curvature extrapolation. Here we simply do a linear extrapolation from inside the real domain to obtain the new boundary block values.

Another option is the zero-order extrapolation where we set the boundary blocks equal to the nearest block within the real domain. For a three-point stencil formulation like that of the staggered upwind scheme and three/five point centered schemes, this has minimal effect on the computations within the real domain. The zero-order extrapolation is our preferred option not

only for its simplicity but also due to its minimal interference with computations within real domain.

Notwithstanding, there are other more elaborate methods for boundary specification that utilize the original mathematical formulations to obtain the boundary block approximations that can be found in the literature (Zhou and Adewumi, 1995; 1996). This formulations allow the boundary blocks estimation to mimic the computations within the real domain thereby maintaining minimal impact on the real domain from boundary condition extrapolation errors.

4.10 Initial Condition

Initial conditions vary depending on the numerical experiment to be run. The idea is to try to mimic the real condition within the pipe at the beginning of the numerical experiment. For instance, in order to model transients observed after a sudden valve shut-in in a natural gas pipeline at steady-state, the steady state solution if first obtained as described in Section 6 and then a valve shut-in effect is applied numerically simply be setting the mass flux (or velocity) at the boundary block to zero. This way, the numerically induced initial condition mimics the actual condition expected within a natural gas pipeline that has achieved steady state condition prior to a valve shut-in.

Chapter 5

Results and Discussions

5.1 Numerical Model Validation

5.1.1 Sudden Valve Shut-in Experiment 1

Before we begin blockage characterization experiments we will demonstrate the accuracy of our transient fluid flow model. For this reason, we reproduce results from a well published experiment in the literature known as the 'line packing' or 'sudden valve shut-in' experiment. In such an experiment, sharp transient propagation is induced by a sudden valve closure on a gas pipeline that had achieved steady state flowing conditions. Tables 5.1 and 5.4 contain fluid and pipeline condition information used in this validation experiment (See Zhou and Adewumi, 1995).

Table 5.1: Data for First Validation Experiment (Eltohami, 1999; Zhou and Adewumi,1995)

Parameters	Data Value
Pipeline Length	30 meters
Pipeline Internal Diameter	0.1 meters
Pipe Roughness	0.03 cm
Gas specific Gravity	0.64
Temperature	80 F
Number of Cell Blocks	300
$InletBoundaryConditions$	
Density	2 $\frac{kg}{m^3}$
Mass Flux	20 $\frac{kg}{m^2 s}$
$OutletBoundaryConditions$	
Density	* $\frac{kg}{m^3}$
Mass Flux at $t = 0^-$	*(≈ 20) $\frac{kg}{m^2 s}$
Mass Flux at $t = 0^+$	0 $\frac{kg}{m^2 s}$

* Calculated from Steady−state Solution

In their work, they derived an analytical solution from the original PDE to determine the steady state solution expected prior to the sudden valve shut-in. They then numerically imposed the effect of a valve shut-in on the natural gas flow at steady state by setting the mass flux at the boundary block originally at 20 $\frac{kg}{m^2 s}$ to zero. The sudden halt in flow at the end of the pipe results in the compression of gases flowing toward the closed valve. As the fluid is compressed, pressure rises due since the pipe is assumed to be rigid. This produces the effect of a sharp transient propagating upstream, opposite the direction of flow. Snap shots of pressure distribution are then recorded at distinct time increments.

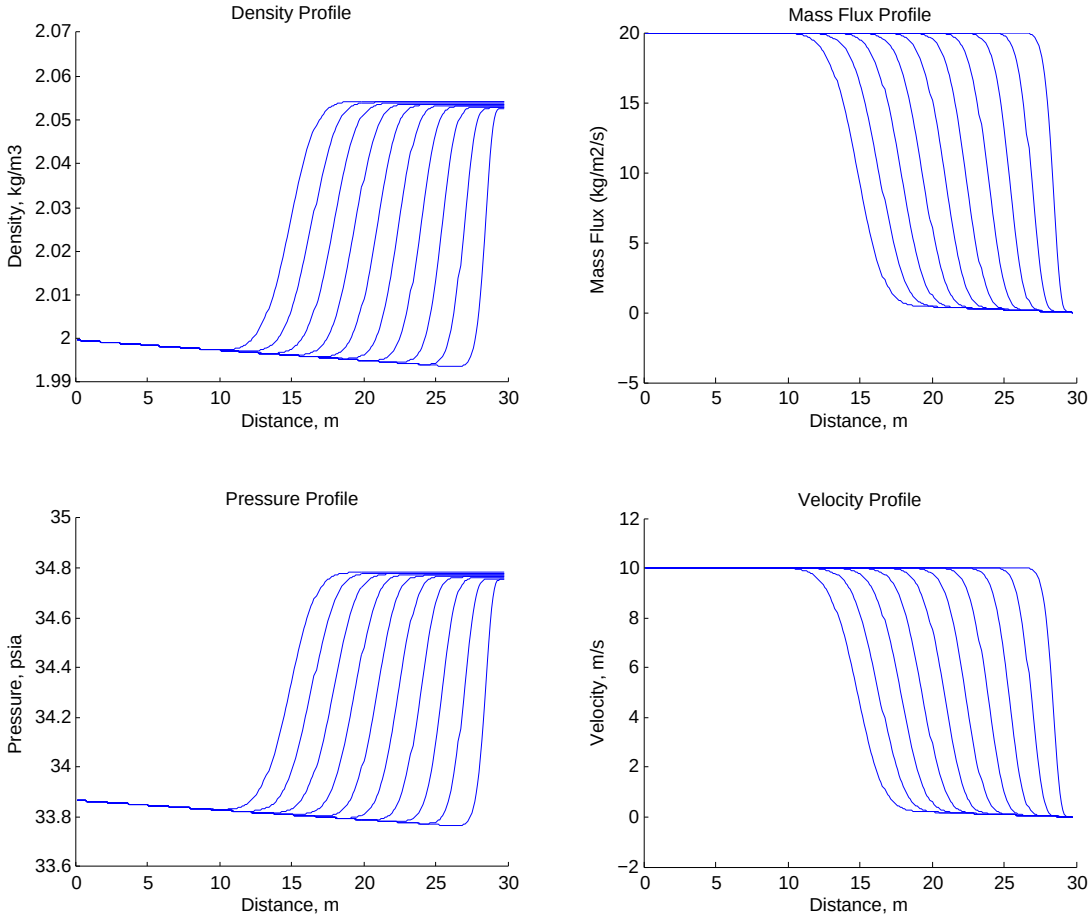

Figure 5.1: Line Parking Validation Experiment 1 (Staggered Upwind Scheme)

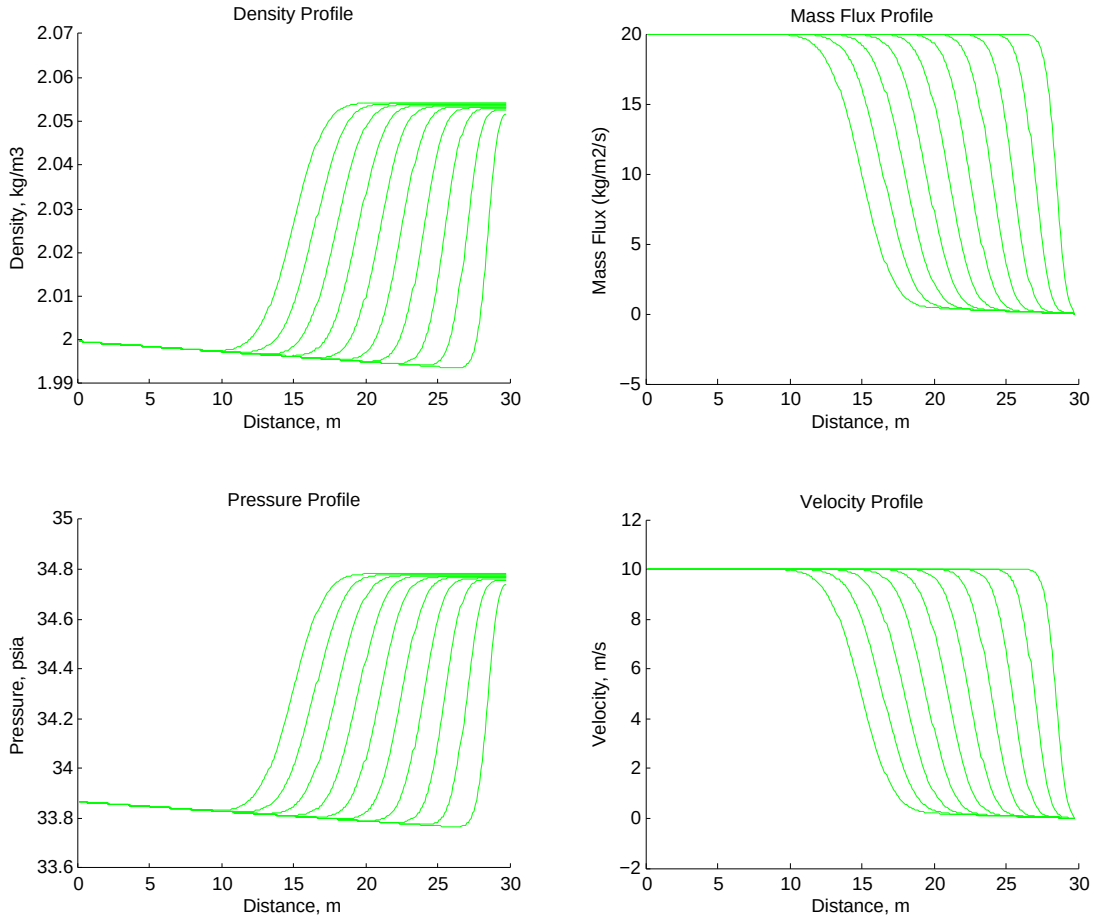

Figure 5.2: Line Parking Validation Experiment 1 (NT centered Scheme)

In order to mimic this scenario, we generate the corresponding steady-state solution as described in section 4.7. This solution is used as the initial condition for the sudden valve shut-in experiment. We then numerically imposed the effect of a sudden valve shut-in by setting the massflux (or velocity) value to zero at the boundary grid cell. The transient response can be observed in Figures 5.1, 5.2 and 5.3.

The numerical experiment was completed using grid cell sizes of 0.1 m and temporal step sizes of 0.5 ms which is larger than the 0.1 ms used in the work of Eltohami (1999) to generate the same result and yet the model was found to be stable. Every transient profile line generated in Figures 5.1, 5.2 and 5.3 are plotted at 4.5 ms intervals. It is important to note that both works (Zhou and Adewumi, 1995; Eltohami, 1999) employed a much more complicated and computationally involved numerical technique than is proposed here.

An important observation is that even though the pressure profile follows the general trend expected, the pressure profile is slightly different from that determined by Eltohami(1999) and

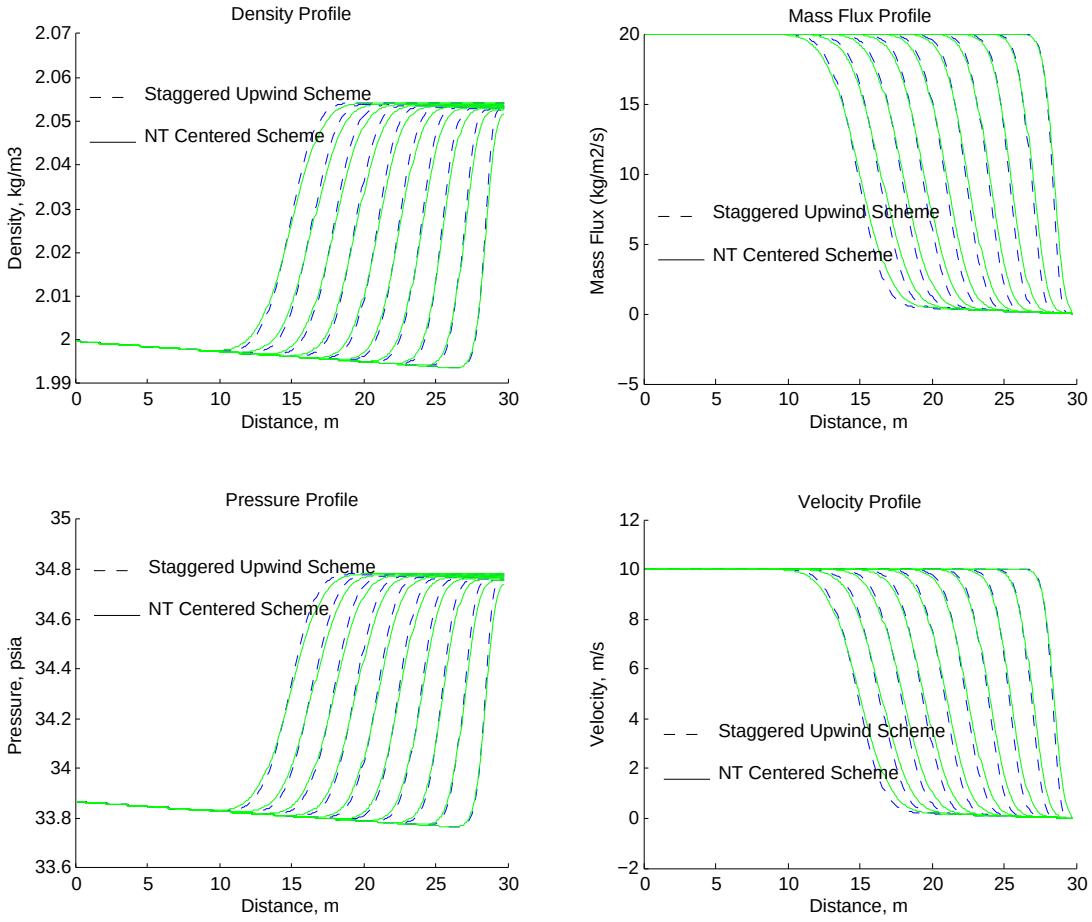

Figure 5.3: Validation Experiment 1

Zhou and Adewumi (1995). The steady state solution shows a pressure shift of about 3.8 psi across the pipe. This difference is due to the slight difference in the estimation of z-factor in both models. In previous works z-factors were estimated using empirical formulations and a gas with standard gravity of 0.64 was used. In this study, the z-factor is estimated using the Peng-Robinson equation of state and the gas composition was deliberately defined in a way that yields standard gravity of 0.64. Notwitstanding, a pressure increase of approximately 1 psi is observed which is in agreement with the work of Zhou and Adewumi (1995) and Eltohami(1999). As expected, the fluid mass flux (or velocity) drops to zero at the outlet due to the sudden valve shut-in and propagates backward. The observed profile agrees with that presented in the works of Zhou and Adewumi (1995) and Eltohami(1999).

A comparison of the results from the staggered upwind scheme and the centered NT scheme can be observed in Figure 5.3. Results from both numerical schemes are very similar however, it is clear that the staggered upwind scheme is provides a sharper wave front than the the centered

Table 5.2: Arbitrary Gas Composition of Approximate standard gravity of 0.64

Component	Percentage Gas Composition
Nitrogen	2.00
Methane	72.99
Ethane	17.95
Propane	5.10
n-Butane	1.10
n-Pentane	0.86

NT scheme.

Table 5.3: Data for Second Validation Experiment (Ibrahim and Adewumi, 1999)

Parameters	Data Value
Pipeline Length	30 meters
Pipeline Internal Diameter	0.3 meters
Pipe Roughness	0.03 cm
Gas specific Gravity	0.64
Temperature	80 F
Number of Cell Blocks	300
InletBoundaryConditions	
Density	$2\ \frac{kg}{m^3}$
Velocity	$10\ \frac{m}{s}$
OutletBoundaryConditions	
Density	$*\ \frac{kg}{m^3}$
Velocity $t = 0^-$	$*(\approx 10)\ \frac{m}{s}$
Velocity $t = 0^+$	$0\ \frac{m}{s}$

* Calculated from Steady-state solution

5.1.2 Sudden Valve Shut-in Experiment 2

Another similar validation experiment with a larger pipe diameter was made to guarantee the accuracy of our numerical model. The work of Ibrahim and Adewumi (1999) which was validated using the analytical solution to the shock tube problem was also reproduced satisfactorily using this model. A similar sudden valve shut-in experiment was conducted, for which the data can be found in Table 5.3. Like the previous validation experiment, initial conditions were obtained

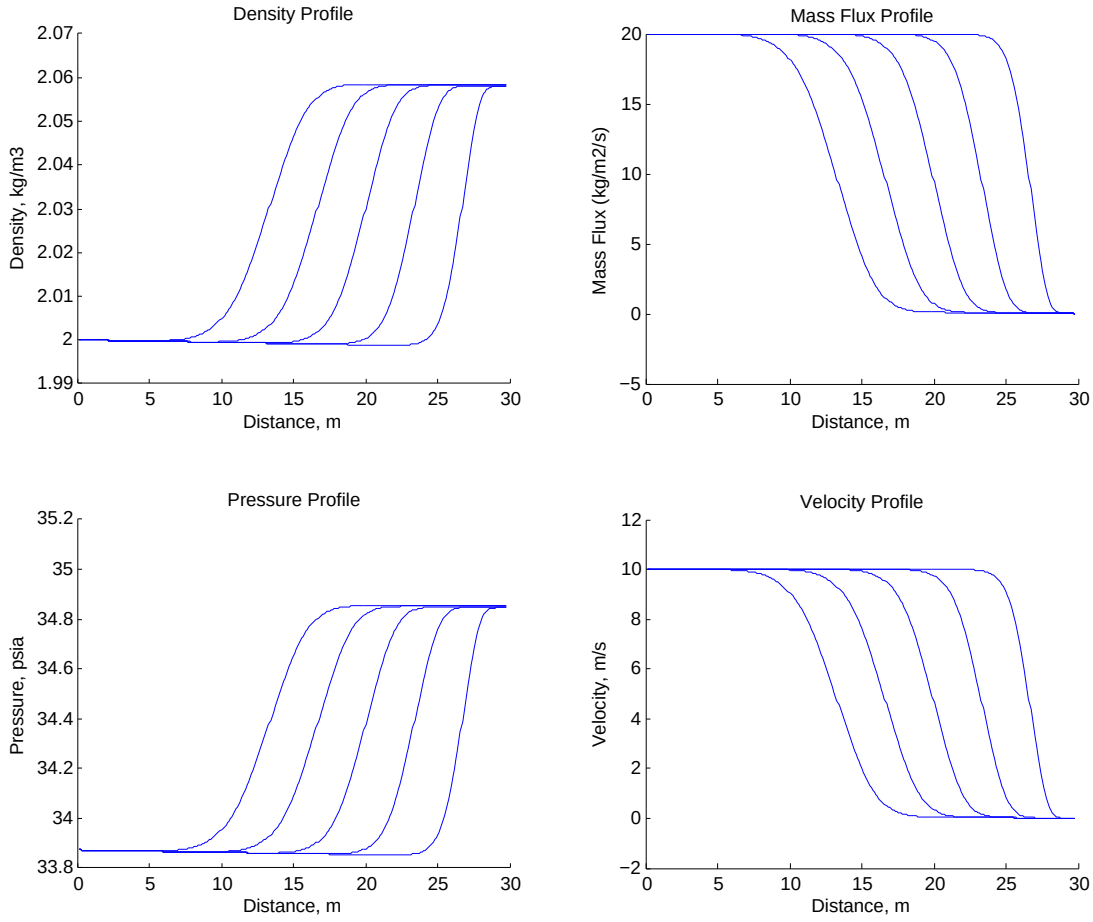

Figure 5.4: Line Parking Validation Experiment 2 (Staggered Upwind Scheme)

from the steady state solution. All numerical experiments performed to simulate this problem was completed using grid cell sizes of 0.1 m and temporal step sizes of 1 ms. The results can be seen in Figures 5.4, 5.5 and 5.6. Every transient profile line in Figures generated in the simulation of this problem are plotted at 10 ms intervals. Like the previous validation, there is an equal shift in the steady state pressure profile across the pipe of approximately 3.8 psia due to the real gas consideration in this study. All other profiles agree with the work of Ibrahim and Adewumi (1999).

5.2 Numerical Experiments

After satisfactorily validating our mathematical model, we tested its blockage detection capacity. Four scenarios modeled in this study are as follows:

- Scenario 1: Gas flow through frictionless pipe without blockage

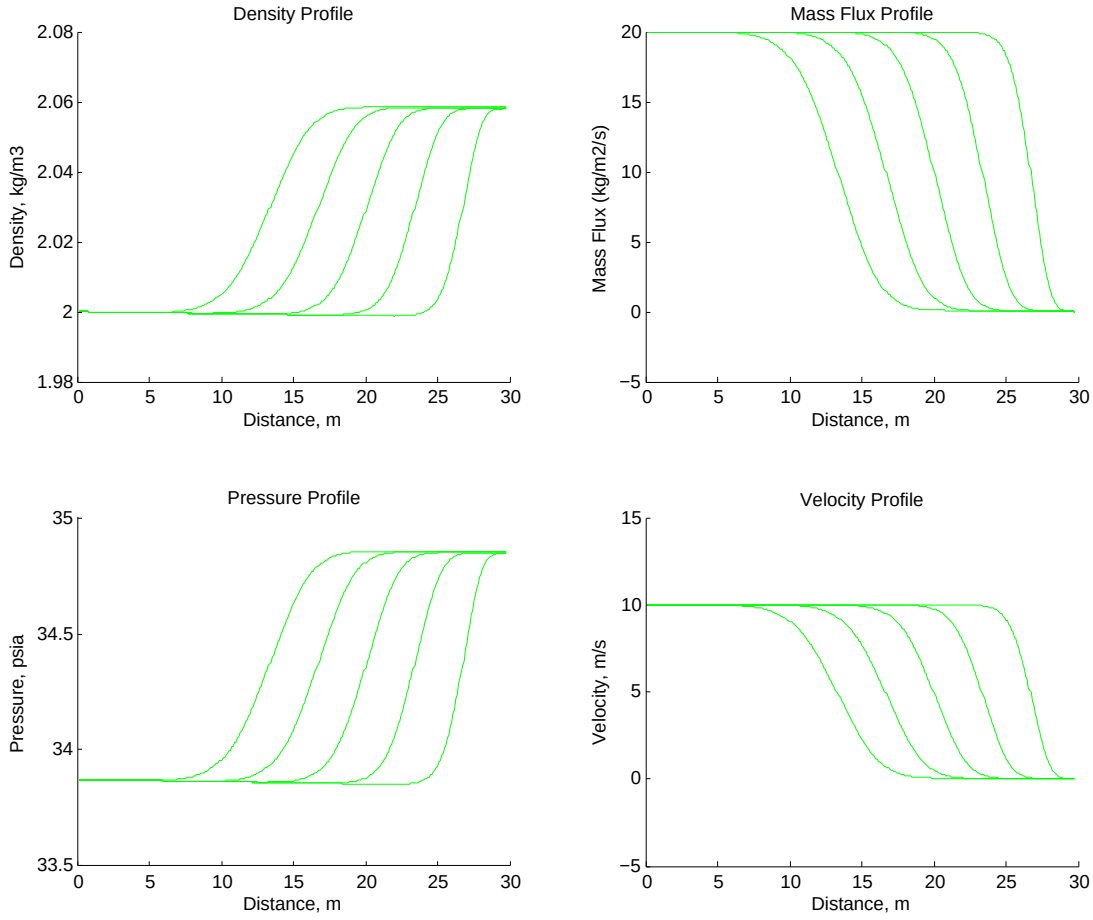

Figure 5.5: Line Parking Validation Experiment 2 (NT centered Scheme)

- Scenario 2: Gas flow through pipe with viscous effects considered without blockage
- Scenario 3: Gas flow through frictionless pipe with partial blockage
- Scenario 4: Gas flow through pipe with viscous effects considered with partial blockage

5.2.1 No Blockage Case: Scenarios 1 and 2

Here we have a natural gas pipeline shut-in at both ends (inlet and outlet boundaries) and allowed to achieve an equilibrium state. Pressure becomes equally distributed across the pipe and flow rate across the pipe goes to zero. A valve at the inlet is then opened and allowed to flow at a constant rate. The valve opening causes a rise in pressure at the inlet (see P_{inc} in Fig. 5.7 and 5.8). The induced pressure wave then propagates along the pipe (see arrow 1 in Fig. 5.9 and 5.10) till it arrives at the boundary. For the frictionless pipe scenario, this incident pressure is maintained constant as the incident wave propagates along the pipe. However, when viscous

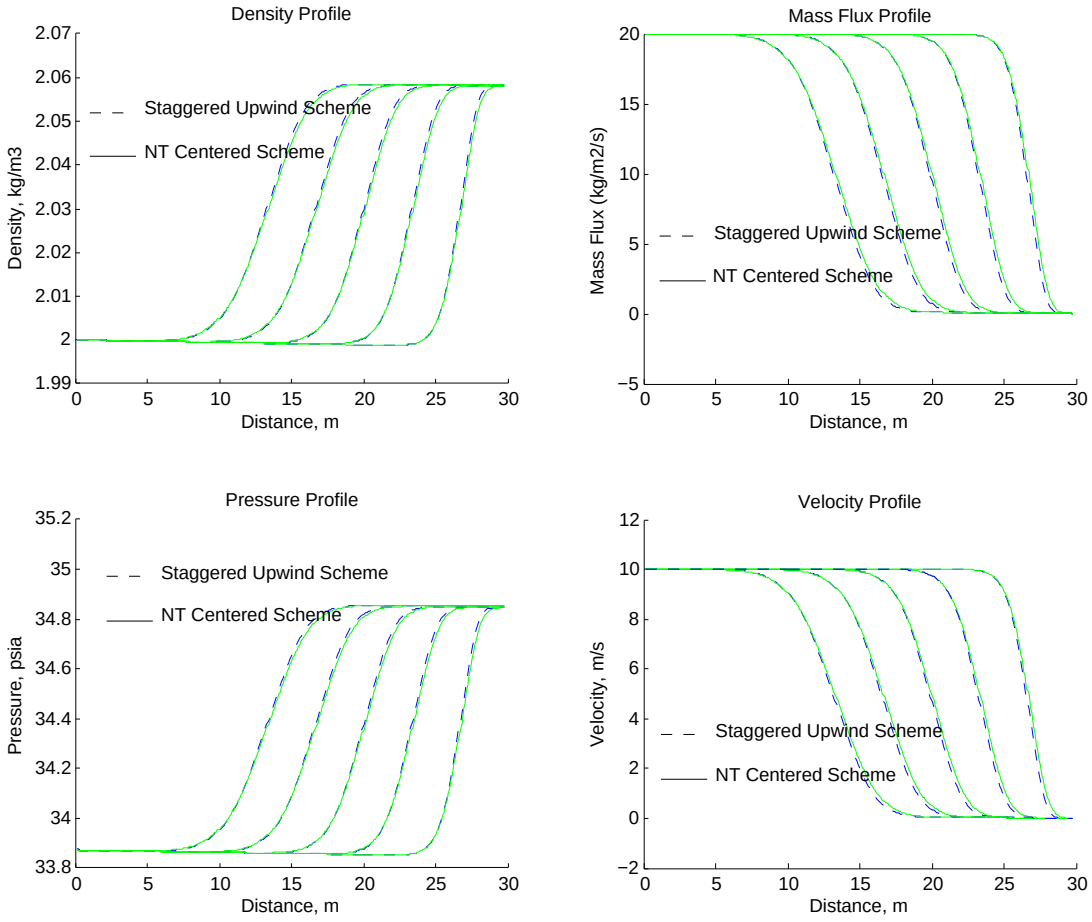

Figure 5.6: Validation Experiment 2

effects are considered, pipe friction deters fluid flow as more gas is pushed along the pipe. As a result, the energy requirement (pressure difference) needed to maintain a constant flow rate at the inlet is higher. For this reason, a continuous rise in inlet pressure is observed as more gas is pushed along the pipe.

Once the pressure wave hits the boundary it is reflected upstream (opposite the direction of fluid flow). See arrow 2 in Figs. 5.9 and 5.10). The pressure wave propagates back upstream with a magnitude twice that of the incident wave. When the wave arrives at the inlet it is reflected back downstream (see arrow 3 in Figs. 5.9 and 5.10) with a magnitude approximately three times that of the original incident pressure (see P_{ref} in Fig. 5.7 and 5.8). Figures 5.11 and 5.12 illustrate the effect of fluid density on the speed of sound.

5.2.2 Partial Blockage Case: Scenarios 3 and 4

5.2.2.1 Continuous Area Change

This experiment is considered for its simplicity as well as the availability of an analytical solution for the reflection of sound energy from linear theory (see Appendix A). To model a sudden continuous area change along a pipe, the diameter of the pipe is reduced from a position x_{start} somewhere along the pipe and the reduced diameter is maintained to the end of the pipe. All necessary transient information needed to characterize a blockage can be obtained from the inlet pressure profile. However, an understanding of the other transient profiles will help in interpreting the inlet pressure profile appropriately. This numerical experiment has also been carried out by Eltohami (1999) and the results follow a similar trend as observed in this study. However, a slight difference is observed in the inlet pressure profile. ΔP_{inc_0} is approximately 0.5 psi lower than that in the work of Eltohami (1999). This difference is attributed to the exclusion of the speed of sound from the momentum equation in this study.

That is:

$$d(x) = \begin{Bmatrix} d_{pipe} & for\ 0 \leq x \leq x_{start} \\ d_{blockage} & for\ x_{start} < x < x_{end} \end{Bmatrix} \tag{5.1}$$

where:
d_{pipe} is the original pipe diameter
$d_{blockage}$ is the blockage diameter
x_{start} is the beginning of the blockage
x_{end} is the end of the blockage(or in this case end of the pipeline)

Like the no blockage case, the pipeline is shut-in at both ends and allowed to achieve equilibrium. The inlet valve is then opened and a constant gas flow is introduced into the system. The pressure wave is induced at the inlet (see P_{inc} in Fig. 5.14 and 5.15). The induced pressure wave then propagates along the pipe (see arrow 1 in Fig. 5.17 and 5.18) till it arrives at the boundary. Like the no-blockage case, this incident pressure is maintained constant as the incident wave propagates along the pipe. However, for the case with viscous effect considered, pipe friction deters fluid flow as more gas is pushed along the pipe. Hence, a continuous rise in inlet pressure

is observed as more gas is pushed along the pipe. Figure 5.13 is a schematic of events that occur as the wave propagates through the partial blockage.

Once the wave hits the partial blockage, some wave is reflected back upstream and the original wave continuous to propagate through the smaller pipe area at a higher magnitude due to fluid compression. See arrow 2a in Fig. 5.17 and 5.18. This compression wave travels back to the inlet and can be observed as P_{ref} in Fig. 5.14 and 5.15. Once the pressure wave hits the boundary it is reflected back upstream opposite the direction of fluid flow (see arrow 3 in Fig. 5.17 and 5.18). The pressure wave propagates back upstream with a magnitude twice that of the incident wave until it arrives back at the partial blockage where an expansion wave (arrow 4) is formed and propagate in both directions (see 4a in Figs. 5.17 and 5.18). When the wave arrives at the inlet it is reflected back downstream (see 5 in Fig. 5.9 and 5.10.

5.2.2.2 Blockage Position Location

Using the input data in Tables 5.2 and 5.4 a sudden area change like that of Fig. 5.16 was imposed on the system. As described before, a pressure wave front is generated at the inlet due to the imposed flow rate at time, $t = 0^+$. Note that the speed of the pressure wave is actually subsonic and can be computed given the distance traveled and how long it takes the wave to return to the inlet. The time corresponding to the inflection point is used to estimate the the actual speed of the wave (calculated as 865.574 $\frac{ft}{s}$ from Fig. 5.14 5.15)under the current fluid and pipe condition. Figure 5.15 shows the rise in pressure from to wave reflection due to the continuous area change. The inflection point of this inlet pressure response is used to estimate distance of the continuous area change from the pipe inlet. Note that the speed of the pressure wave is essentially unaffected by friction and is realistically assumed constant as it propagates from the inlet to the outlet and back.

Therefore,

$$x_{start} = \frac{c \times t_{ref}}{2} \tag{5.2}$$

where:

c = averaged speed of sound in the pipe (OR actual wave speed).

t_{ref} = the time it takes for the reflected wave to reach in inlet.

5.2.2.3 Blockage Severity Determination

The severity of the blockage is estimated through an area ratio, $\frac{A}{A_{pipe}}$ prediction. The analytical expression for the area ratio can be found in Appendix-A and a full derivation of the equations can be found in the work of Ahmed (1996) or Adewumi et al (2000). Note that the pressure reflection ratio (R_p) is calculated as shown in equation 5.3 instead to account for the effect of friction:

Table 5.4: Experiment 1: Continuous Area Change

Parameters	Data Value
Pipeline Length	1 mile
Pipeline Internal Diameter	8 inches
Pipe Roughness	0.0006
Temperature	80 F
Number of Cell Blocks	200
x_{start}/L	0.64
Area Ratio	0.64
InletBoundaryConditions	
Pressure	1000 psia
Flowrate(Q) at $t = 0^-$	0 MMSCFD
Flowrate(Q) at $t = 0^+$	10 MMSCFD
OutletBoundaryConditions	
Pressure	1000 psia
Flowrate(Q) at	0 MMSCF $\frac{m}{s}$

$$R_p = \frac{\Delta P_{ref_b} - \Delta P_{inc0}}{\Delta P_{inc0} + \Delta P_{fric}} = \frac{\Delta P_{ref_b} - \Delta P_{inc0}}{\Delta P_{inc}} \tag{5.3}$$

where:

R_{pinlet} is the pressure reflection ratio at the inlet.

P_{ref_b} is the blockage reflection inlet pressure response.

P_{inc} is the incident inlet pressure response right before the block.

P_{inc0} is the incident inlet pressure response induced by a constant flowrate.

ΔP_{fric} is the pressure increase due to frictional force.

$\Delta P_{fric} = \Delta P_{inc}$ - ΔP_{inc0}

$\Delta P_{ref} = P_{ref}$ - P_o

$\Delta P_{inc} = P_{inc}$ - P_o

$\Delta P_{inc_0} = P_{inc_0}$ - P_o

P_o is the original pressure prior any pulse induction on the system.

Table 5.5: Inlet pressure data for Blockage Severity Prediction

Parameter	Frictionless Pipe	Real Pipe
P_0 (psia)	1000	1000
P_{inc_0} (psia)	1003.5	1003.5
P_{inc} (psia)	1003.5	1004.1
P_{ref_b} (psia)	1005	1005.4
ΔP_{inc_0} (psia)	3.5	3.5
ΔP_{inc} (psia)	3.5	4.1
ΔP_{ref_b} (psia)	5	5.4
R_p (Old Formulae)	0.42857	0.54286
R_p (New Formulae)	0.42857	0.46341

Table 5.6: Continuous Area Change Location and Severity Prediction

Parameter	Predicted	Actual	Abs. Percentage Error
Blockage Location			
FrictionlessPipe			
Using speed of sound (980 ft/s)	3,567 ft	3168	12.60 %
Using actual wave speed (865.6 ft/s)	3151 ft	3168	0.54 %
ConsideringFriction			
Using speed of sound (980 ft/s)	3,567 ft	3168	12.60 %
Using actual wave speed (865.6 ft/s)	3151 ft	3168	0.54 %
Blockage Severity			
FrictionlessPipe			
Using Old Formulae	0.647	0.64	1.1 %
Using New Formulae	0.647	0.64	1.1 %
ConsideringFriction			
Using Old Formulae	0.573	0.64	10.5 %
Using New Formulae	0.624	0.64	2.5 %

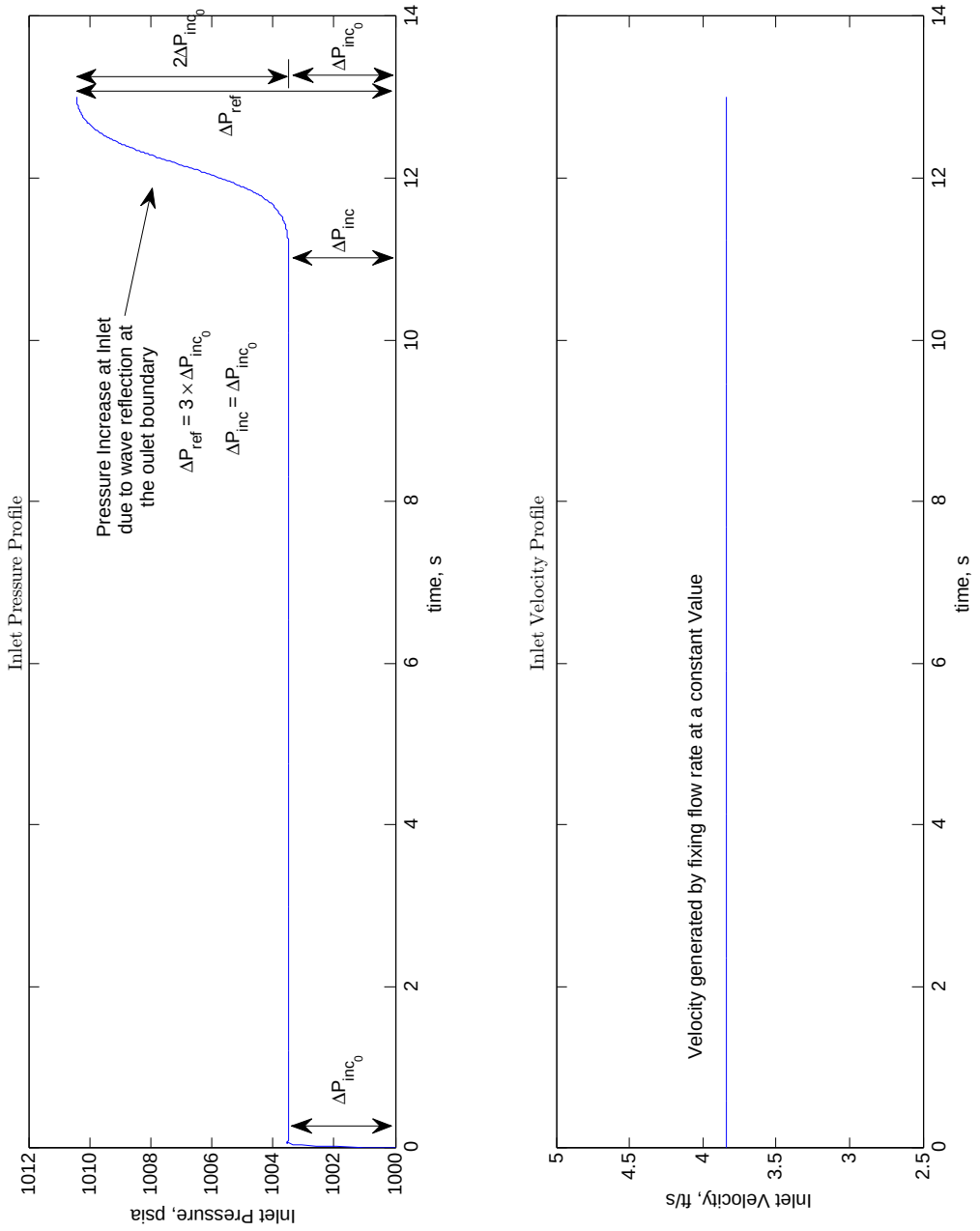

Figure 5.7: Inlet Pressure Profile (IN FRICTIONLESS PIPE)

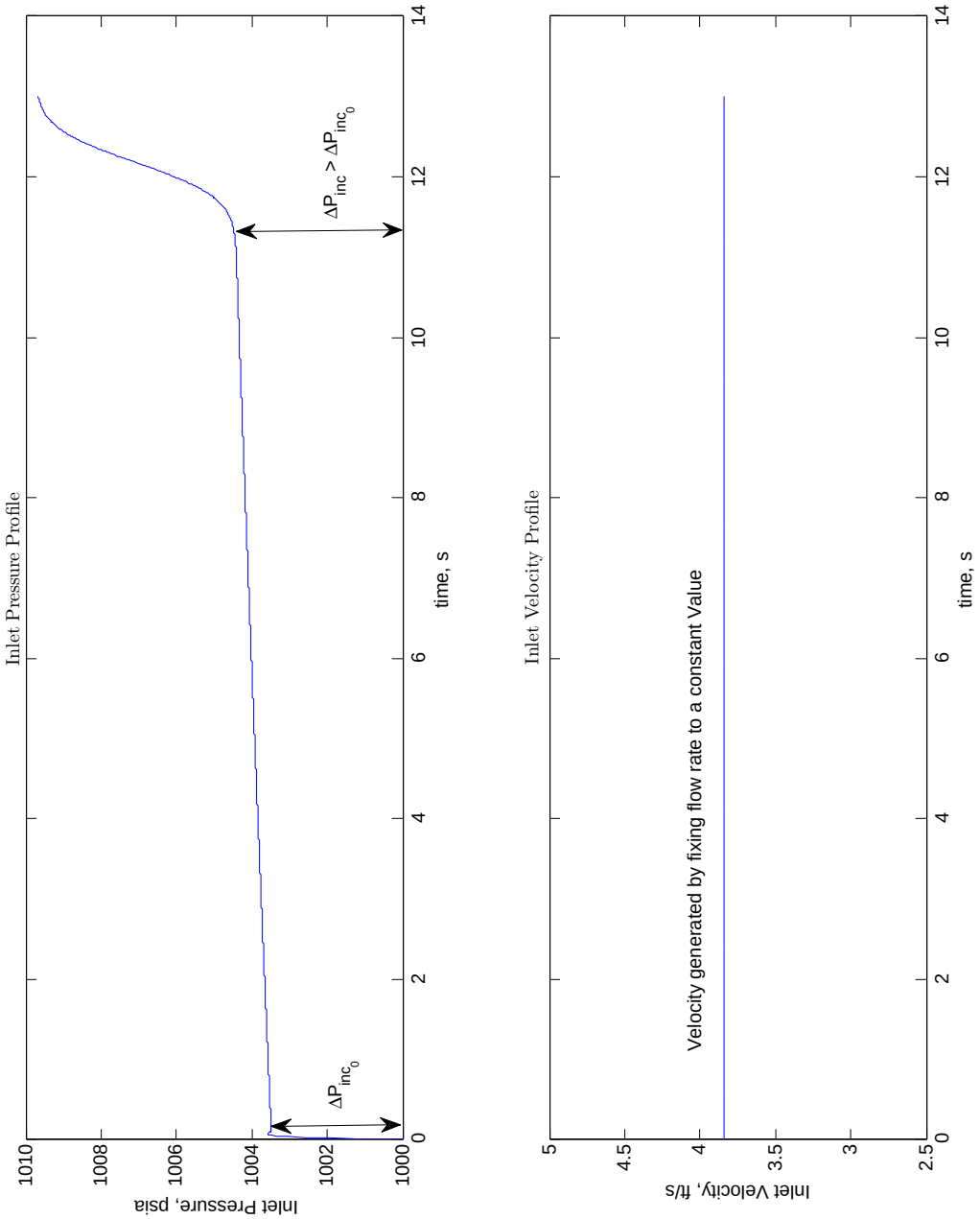

Figure 5.8: Inlet Pressure Profile (WITH FRICTION)

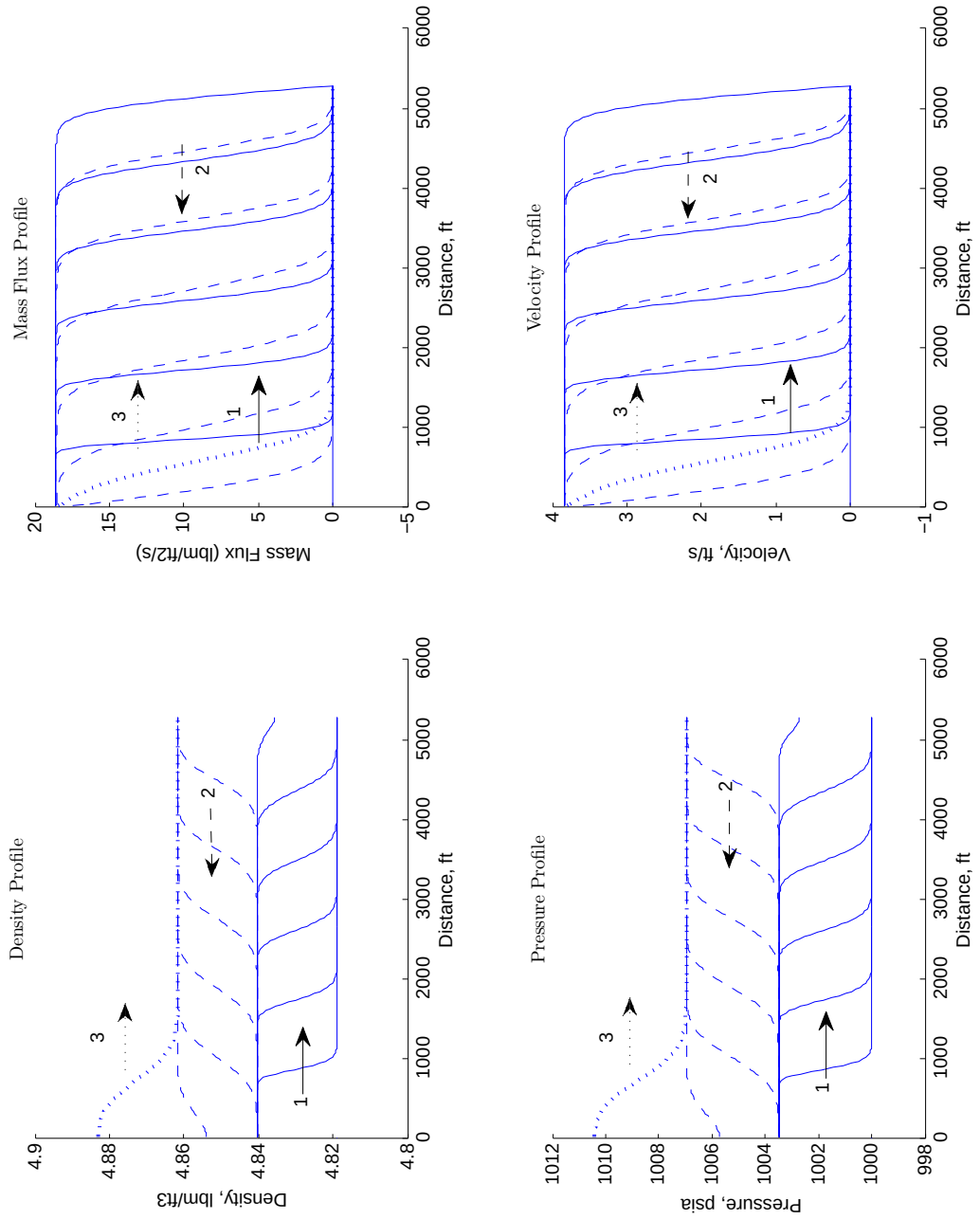

Figure 5.9: Transient Profiles (IN FRICTIONLESS PIPE)

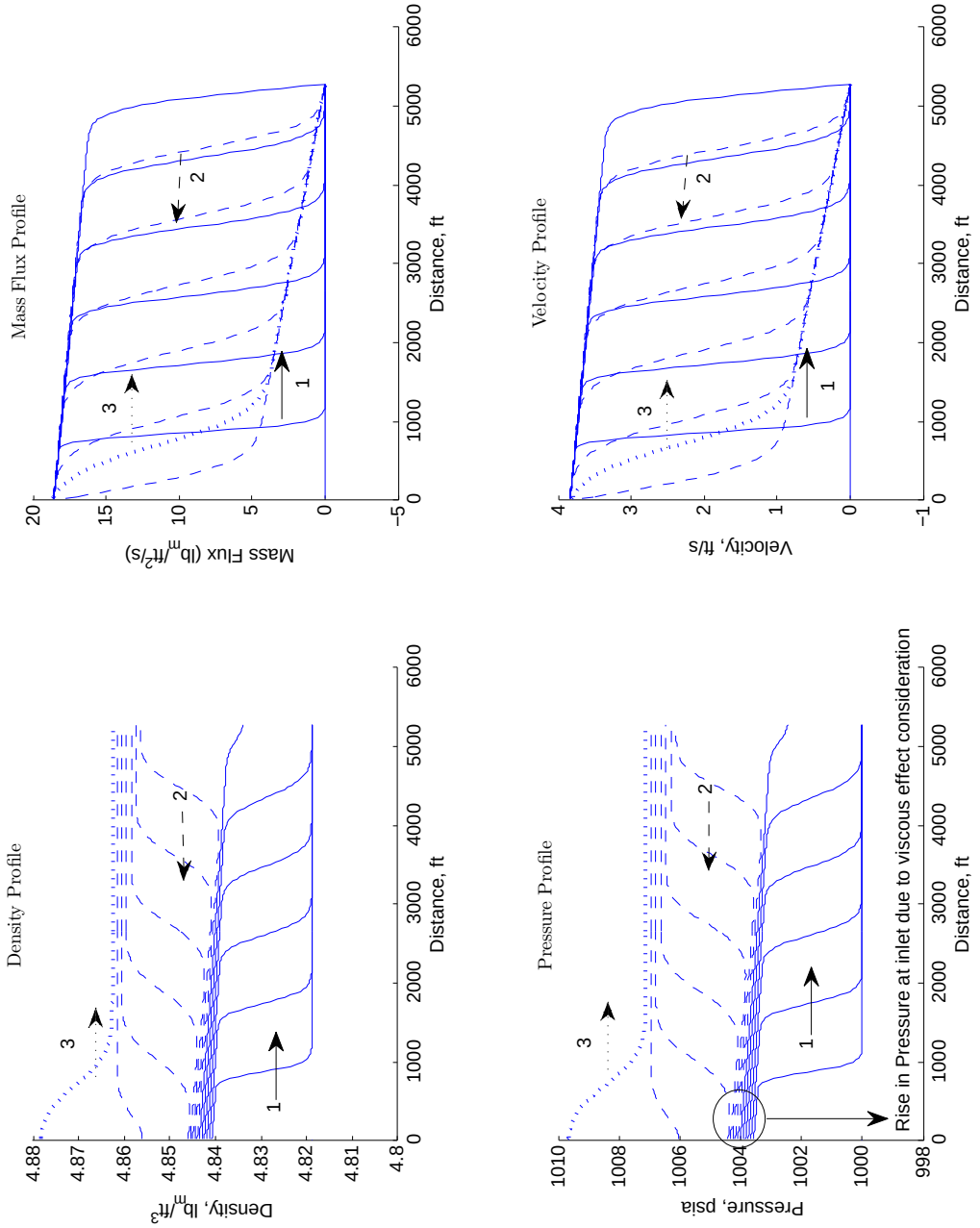

Figure 5.10: Transient Profiles (WITH FRICTION)

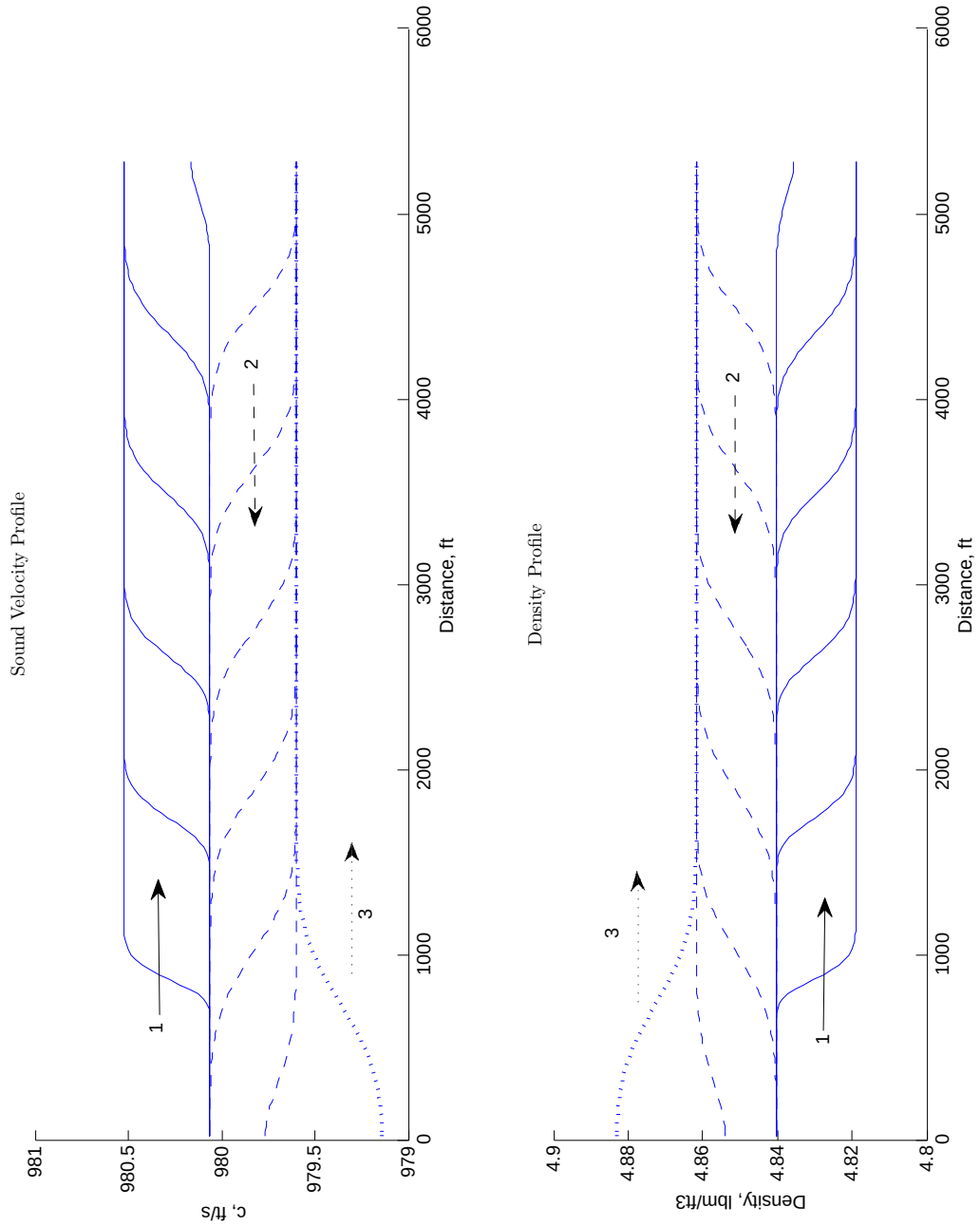

Figure 5.11: Speed of Sound and Density profiles (IN FRICTIONLESS PIPE)

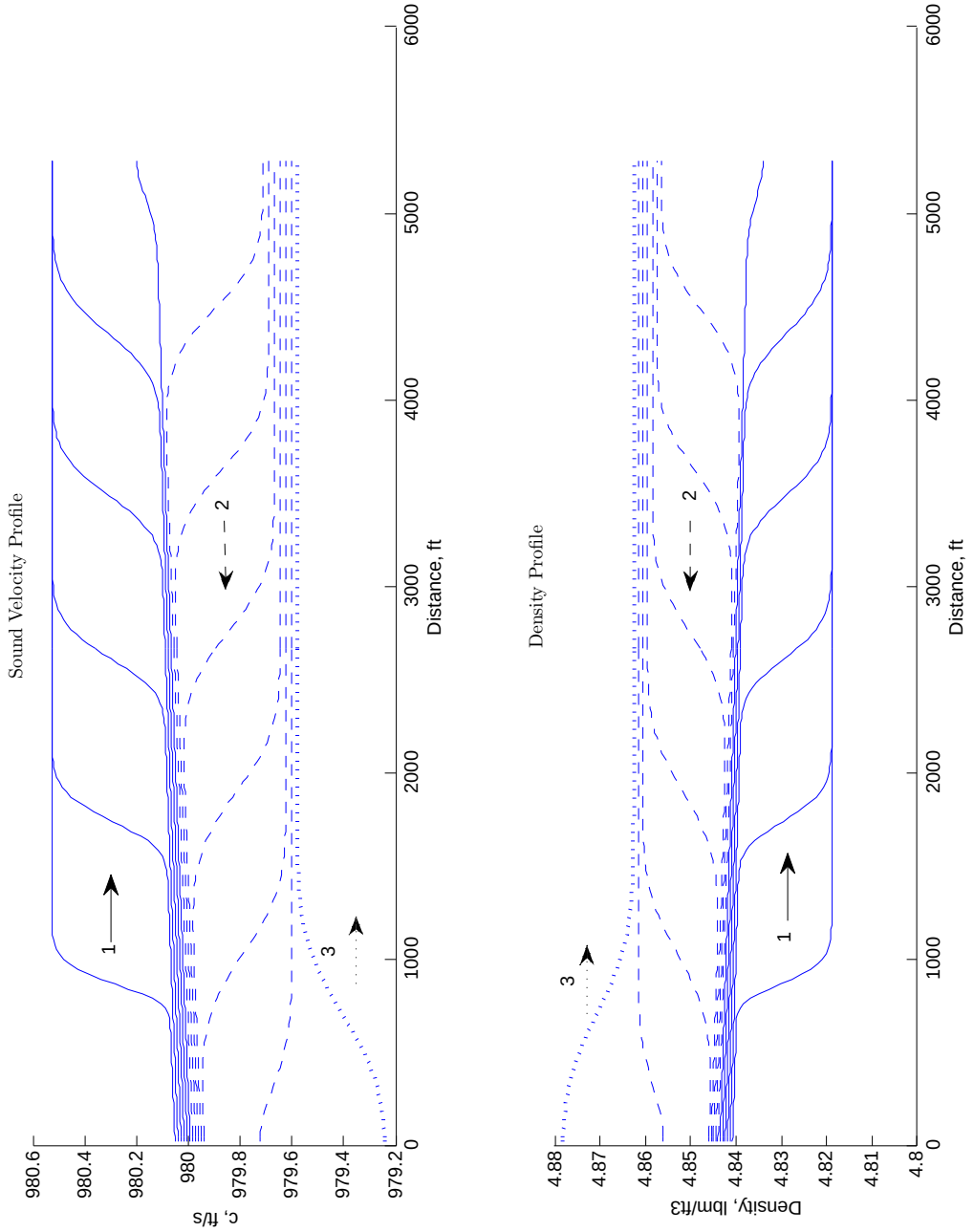

Figure 5.12: Speed of Sound and Density profiles (WITH FRICTION)

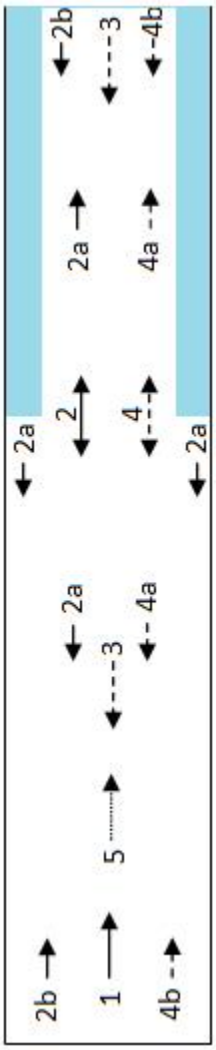

Figure 5.13: Schematic of events generating expansion and compression pulses

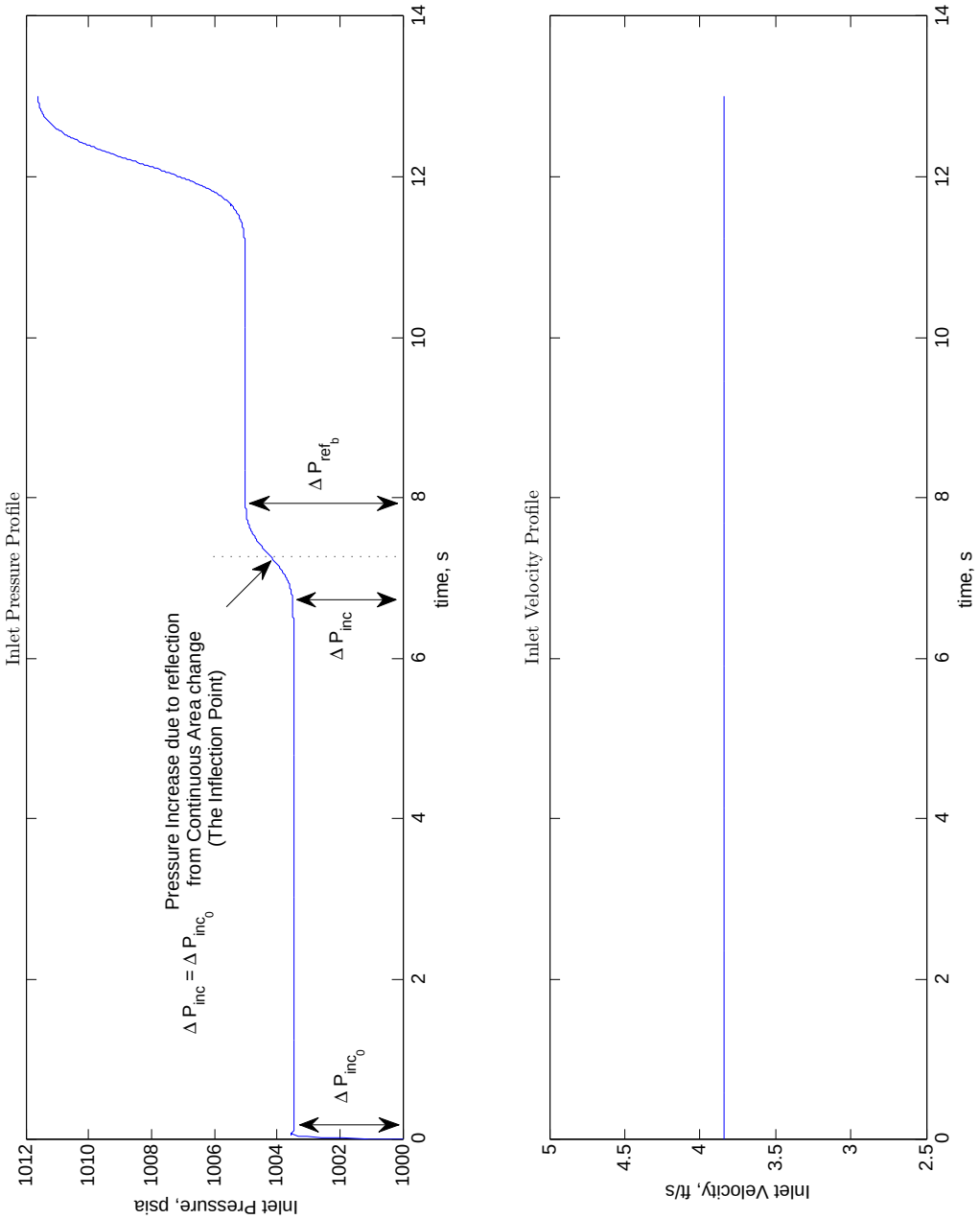

Figure 5.14: Continuous Area Change Experiment; Inlet Pressure Profiles (NO FRICTION)

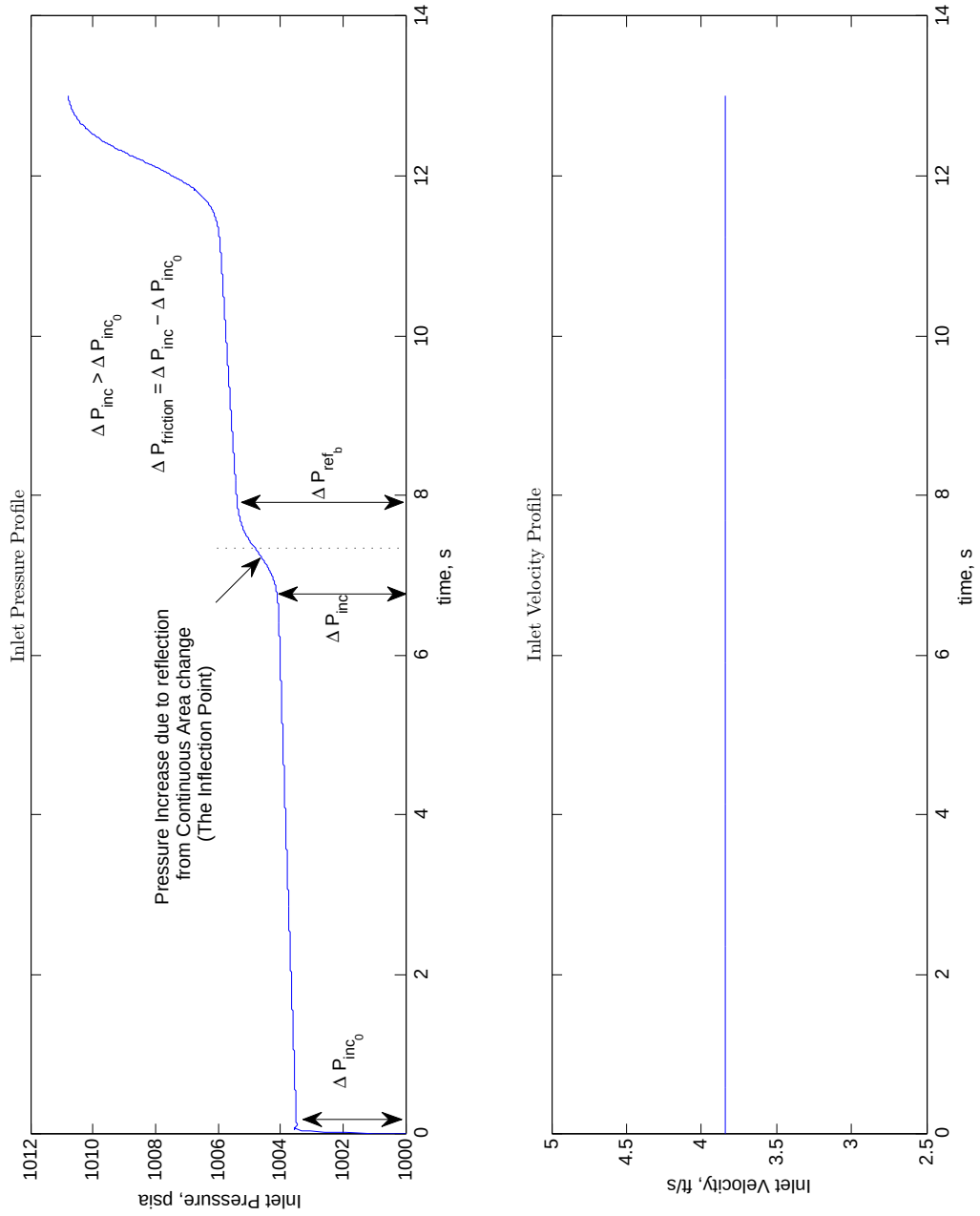

Figure 5.15: Continuous Area Change Experiment; Inlet Pressure Profiles (WITH FRICTION)

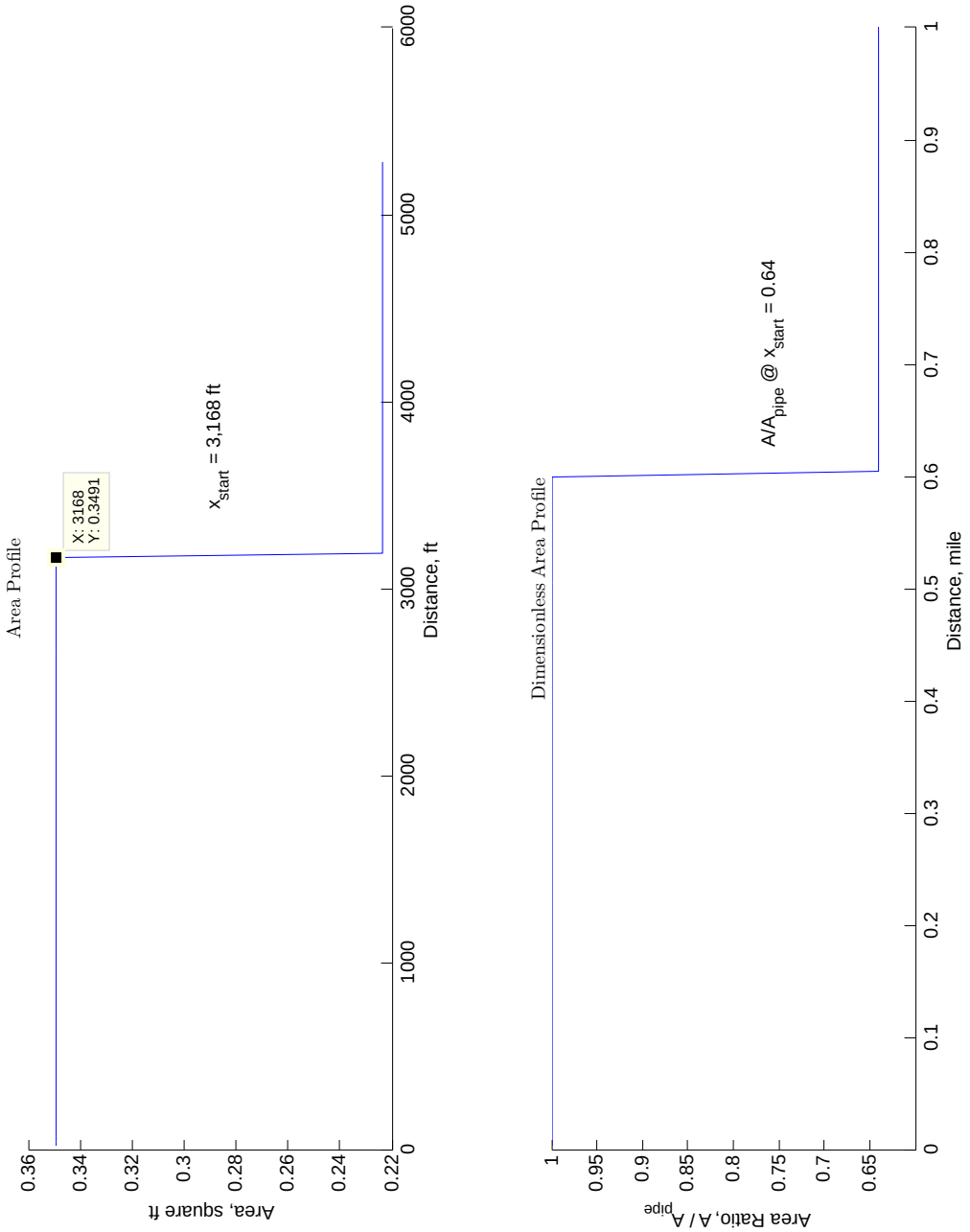

Figure 5.16: Continuous Area Change Experiment; Area Profile

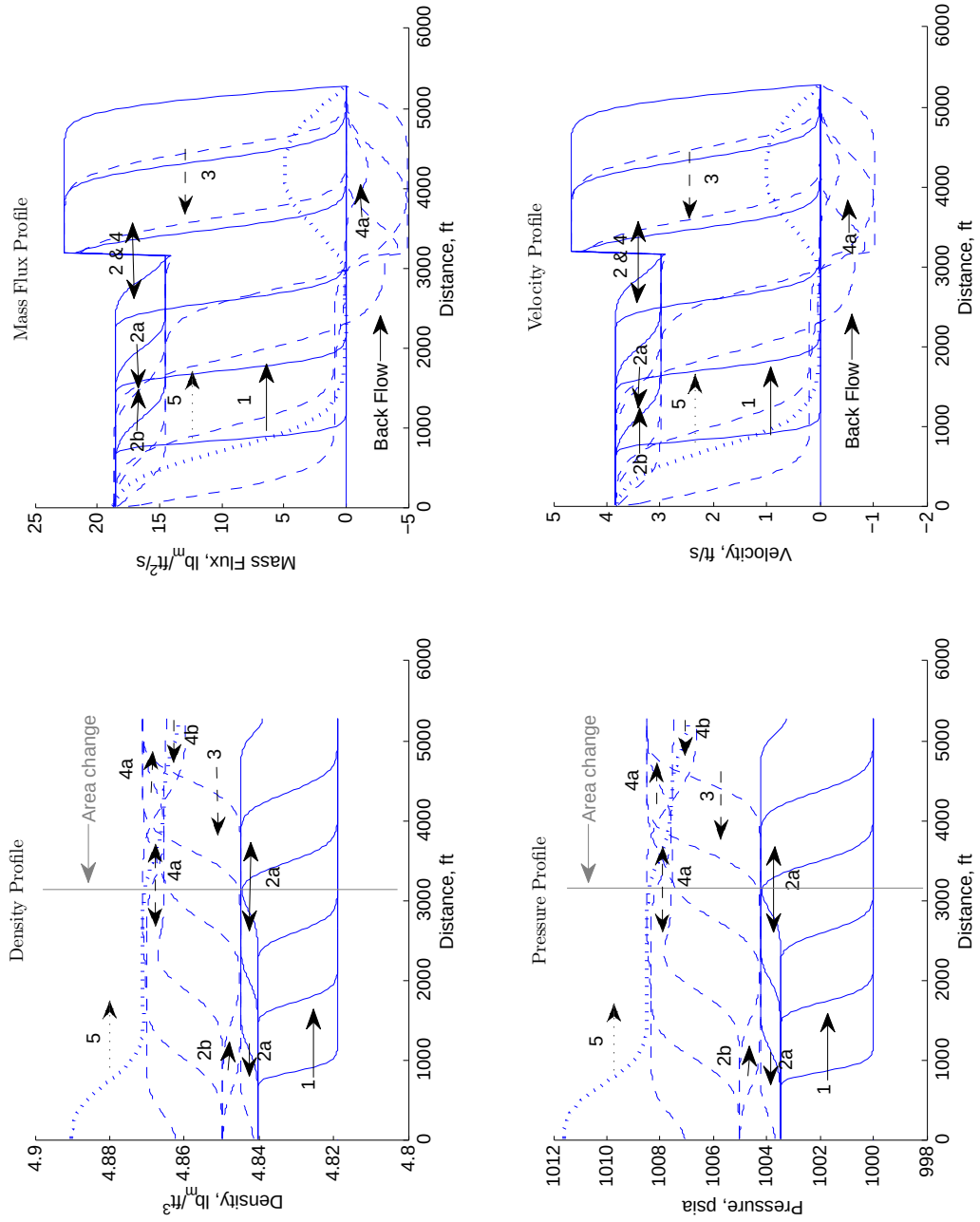

Figure 5.17: Continuous Area Change Experiment; Transient Profiles (NO FRICTION)

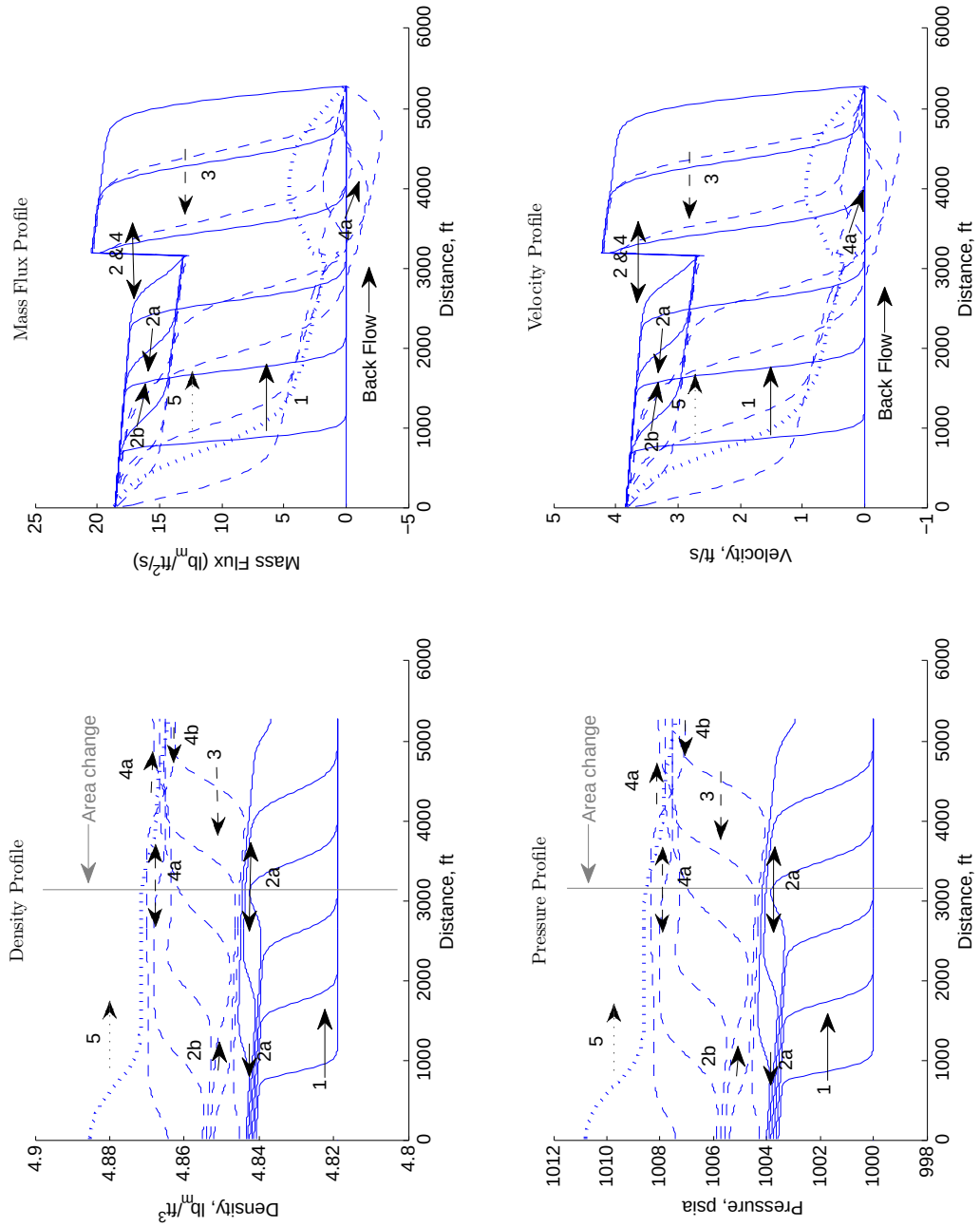

Figure 5.18: Continuous Area Change Experiment; Transient Profiles (WITH FRICTION)

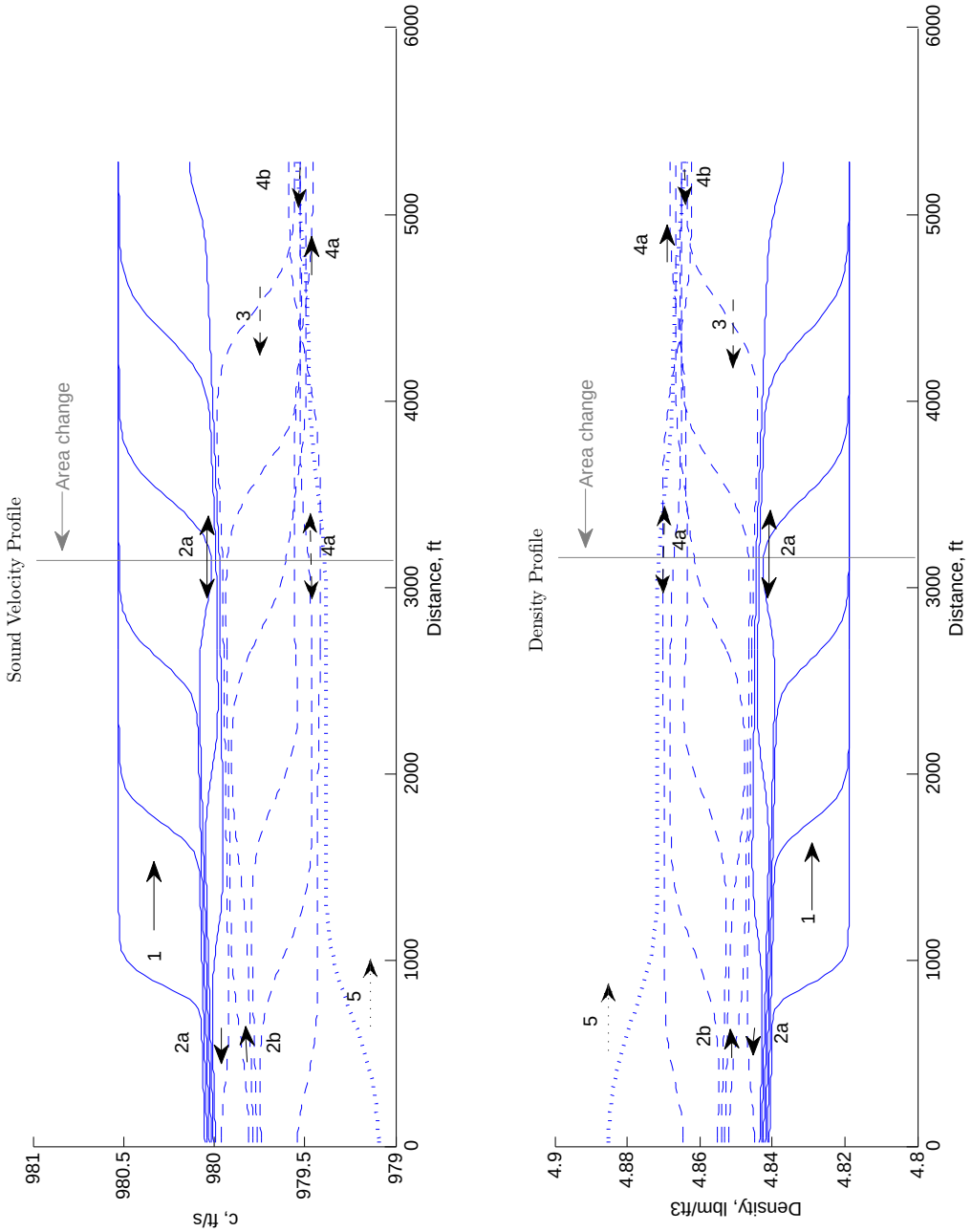

Figure 5.19: Continuous Area Change Experiment; Speed of Sound and Density Profiles (WITH FRICTION)

Chapter 6

Conclusion

We have developed a simple yet fast and robust numerical technique that accurately captures transient flow in natural gas pipelines and suitable for blockage characterization. The model has been utilized for blockage characterization and was found to be stable in the presence of domain discontinuities. The numerical model was compared to the works of Zhou and Adewumi (1995) and Ibrahim and Adewumi (1999) and was found to show a similar level of accuracy as one would expect from more complicated numerical methods. The model was also found to be stable for relatively large time steps as a result of the fully-implicit solution approach. Furthermore, the compression wave fronts generated in this study were similar to that of first and second order TVD schemes (see Ibrahim and Adewumi, 1999).

Additionally, there was no need for prior estimation of wave speed before numerical experiments since the assumption of pressure waves propagating at the speed of sound was not made it this study. The wave speed is computed from inlet pressure transient profile data generated from the numerical experiments. Using the actual wave speed to predict blockage location reduced blockage location prediction error by one order of magnitude. The speed of sound was not incorporated into the flux terms in our mathematical formulation of the problem hence analysis of inlet pressure data using speed of sound for blockage location showed that the sonic speed wave propagation assumption does not provide accurate estimates for the position of blockages along a pipe (12 % error). But when the wave speed is computed based on the knowledge of the length of the pipe and how long it takes for the induced pressure wave front to return to the inlet after its reflection from the outlet boundary, the position of the artificial blockage is accurately predicted (0.54 % error).

Previous studies (Adewumi et al., 2000 and 2003) were completed with descent blockage characterization by neglecting viscous effects in their numerical experiments. Evaluation of the effect of friction on blockage characterization shows that friction significantly reduces the accuracy of blockage severity prediction but has no measurable effect on the prediction of the blockage location. Blockage severity analysis was improved by a modification of the pressure reflection

ratio equation to account for the effect of friction on the inlet pressure profile. If viscous effects are considered in the numerical experiments, blockage severity was found to be under predicted by about 10 % using the old equations. But using the new equation severity is over predicted by about 7 %. If viscous effects are neglected in the numerical experiments, both equations collapse to the same and severity prediction error reduces to 1.1 %. However, this is not practical.

The NT centered TVD scheme was found to be unstable upon introduction of a discontinuity into the domain in the form of the artificial blockage. Hence only the staggered upwind scheme was used for blockage detection and characterization. The quasi compositional model required a generic set of composition with equivalent gas standard gravity in order to validate the model with precious studies and yet validation results were satisfactory.

Chapter 7

Recommendation

Some improvements can still be made to the new model. The temporal resolution used in this study is a simple first-order implicit finite difference approximation of the time derivatives from the conservation equations, also known as the backward Euler method. Hence the smearing of the wave fronts over time. The use of higher order approximations such as the implicit 4th-order Runge-Kutta method or a higher order variation of the Adams method for the time derivative will greatly improve the accuracy of the solution over time. Also the simple upwind finite volume scheme used could be upgraded to a higher order TVD scheme with flux-limiters. This will improve the spacial resolution of the gas-dynamic model. See Ibrahim and Adewumi (1999).

Blockage severity prediction can be improved by accurately and quantitatively accounting for the effect of friction in inlet pressure data analysis. Additionally, the assumption that gas compression waves propagates at the speed of sound is inaccurate for natural gas flow. Furthermore, the isothermal system assumption is far-fetched due to the fact that temperature variations in a pipelines are too large to be considered negligible. However, this will make the problem more difficult since it implies that we will need to integrate a thermodynamic model to the gas-dynamic model to account for changes in the internal energy of the system. In order to have a more practical model, all of the assumptions of ideality must be discarded.

Additionally, instead of assuming an artificial blockage, phase behavior modeling can be used to determine the conducive states for the formation of hydrates. The phase behavior model can then be coupled with the gas-dynamic model. However, this will require a proper understanding of particle distribution in fluid flow. Altimately, the model can be made more practical for use in the area of flow assurance in natural gas pipelines as well as sub-sea production facilities.

Appendix A

THEORETICAL EXPRESSIONS FOR SEVERITY DETERMINATION

A.1 Continuous Area Change

Equation A.1 is an analytical expression that describes blockage severity (or pipe area ratios) as derived for a plane wave propagating in a pipe of cross-sectional area A_1 and entering a second pipe of area A_2 (See Ahmed, 1996). The following assumptions are made in the development of the analytical expression:

1. No wave is reflected from the far end of the second pipe with area, A_2.
2. The wave length is large compared to the diameter of both pipes.

$$\frac{A_2}{A_1} = \frac{1 - \frac{R_p}{2}}{1 + \frac{R_p}{2}} \tag{A.1}$$

$$R_p = \frac{\Delta P_{ref_b} - \Delta P_{inc_0}}{\Delta P_{inc_0}} \tag{A.2}$$

where:
R_p is the pressure reflection ratio at the inlet.
P_{ref_b} is the reflected pressure response due to a partial blockage observed at the inlet.
P_{inc_0} is the incident pressure response due to an induced flowrate observed at the inlet.
$\Delta P_{ref_b} = P_{ref_b}$ - P_o
$\Delta P_{inc_0} = P_{inc_0}$ - P_o
P_o is the original pressure prior any flow pulse induction on the system.

Appendix B

Equation of State: Peng and Robinson, 1976

$$P = \frac{R\,T}{V_m - b} - \frac{a\,\alpha}{V_m^2 + 2bV_m - b^2} \tag{B.1}$$

$$a = \frac{0.45724\,R^2\,T_c^2}{p_c} \tag{B.2}$$

$$b = \frac{0.07780\,R\,T_c}{p_c} \tag{B.3}$$

$$\alpha = \left(1 + \left(0.37464 + 1.54226\,\omega - 0.26992\,\omega^2\right)\left(1 - T_r^{0.5}\right)\right)^2 \tag{B.4}$$

$$T_r = \frac{T}{T_c} \tag{B.5}$$

In Polynomial Form:

$$Z^3 - (1 - B)\,Z^2 + (A - 3B^2 - 2B)\,Z - (AB - B^2 - B^3) = 0 \tag{B.6}$$

$$A = \frac{a\alpha p}{R^2 T^2} \tag{B.7}$$

$$B = \frac{bp}{RT} \tag{B.8}$$

Appendix C

Effect of Time Step Size on Solution Accuracy

Since the backward Euler method was used to discretize the time derivative the numerical model is unconditionally stable. However, convergence is not the only criteria for applicability of a numerical technique. Another criteria is the ability of the numerical model to accurately represent the actual physical phenomena. Parameters such as the combination of the magnitude of the time step and the grid cell sizes have a notable influence on the accuracy of the solution. The magnitude of the time step used (Δt) is dependent upon the size of the grid cell (Δx). Hence, we will be concerned about the size of lamda (λ).

$$\lambda = \frac{\Delta t}{\Delta x} \tag{C.1}$$

We will use the numerical experiment for blockage characterization documented in the results section to illustrate the effect of the magnitude of λ on the accuracy of the solution. In this experiment, Δx was set to 26.4 feet (i.e. 200 segments in a mile long pipe) and Δt was varied. The results can be observed in the plots below. Figures C.1, C.2 and C.3 all show pressure and velocity profiles. We can observe that for λ = 3.7878E-5 (Fig. C.1) the shock front is sharp, however, there is significant numerical dispersion. However, for λ = 3.7878E-4 the result appears smoother. And finally, for λ = 3.7878E-3, the solution is too damp and the shock front is smeared. Similar effects can be observed on the inlet pressure profile data over time. See Figures C.4, C.5 and C.6

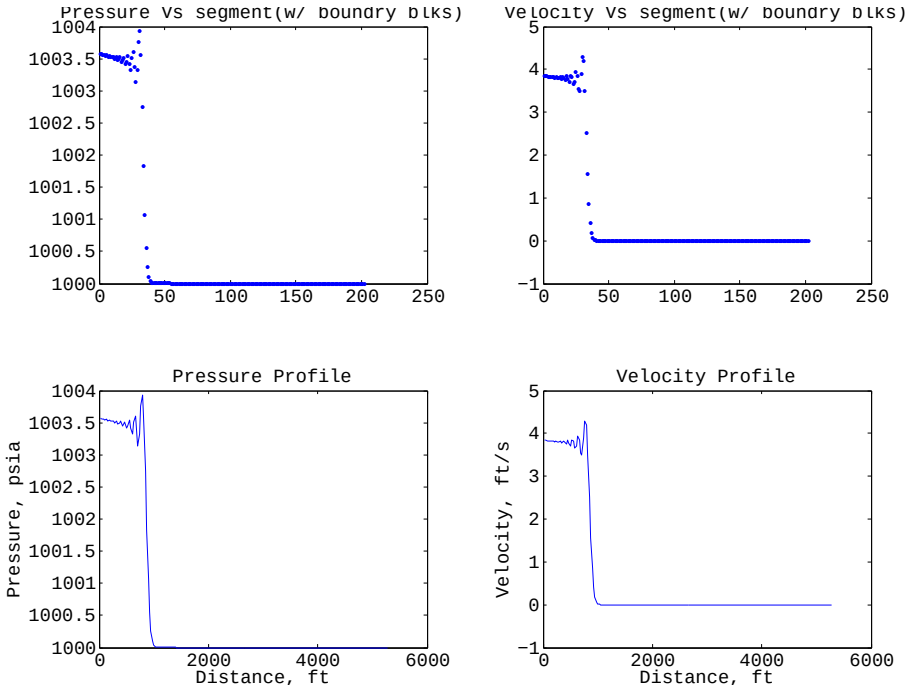

Figure C.1: Pressure and Velocity Profile for λ = 3.7878E-5

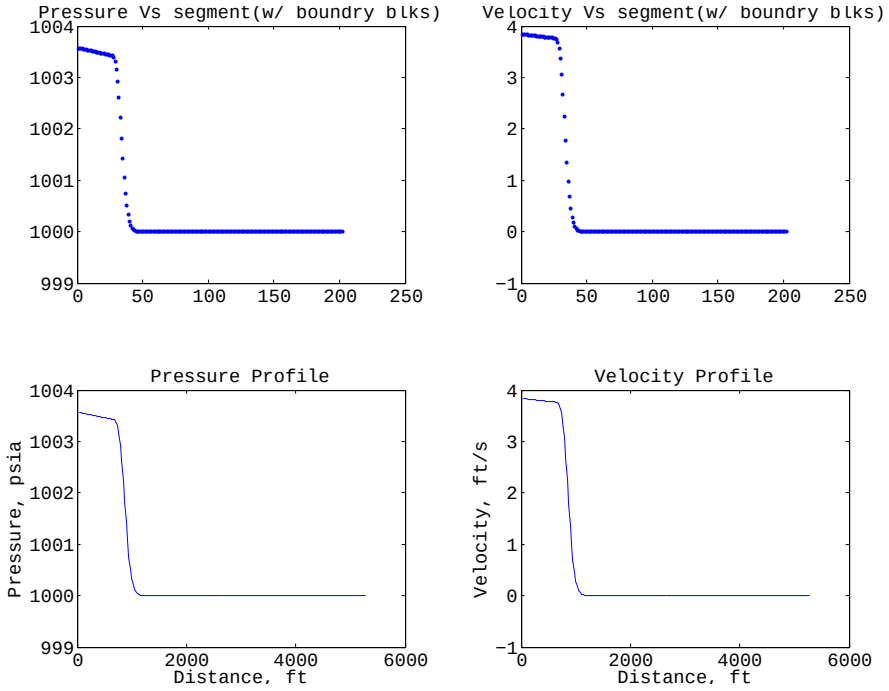

Figure C.2: Pressure and Velocity Profile for λ = 3.7878E-4

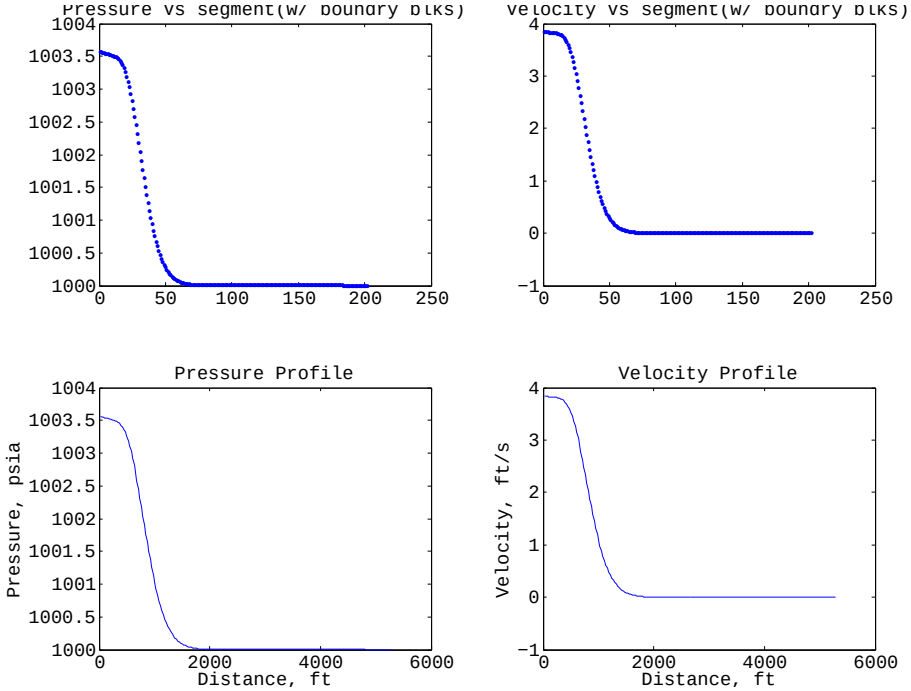

Figure C.3: Pressure and Velocity Profile for λ = 3.7878E-3

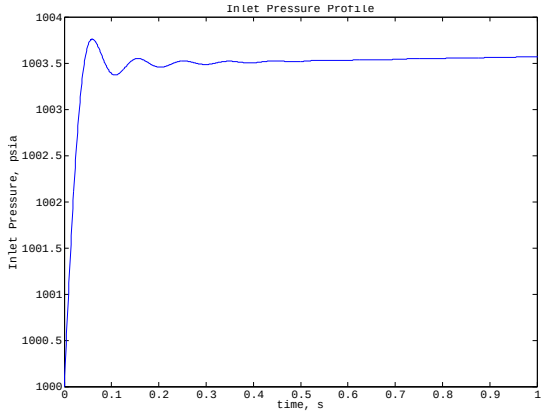

Figure C.4: Inlet Pressure Profile for λ = 3.7878E-5

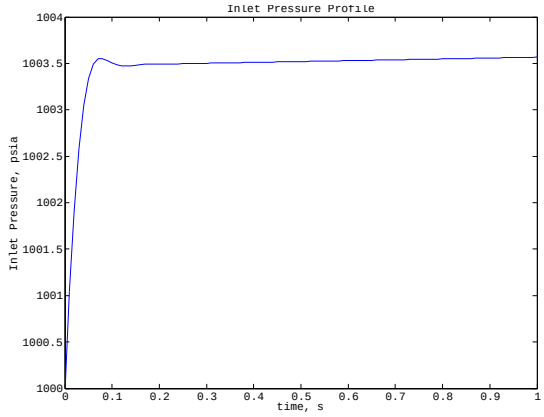

Figure C.5: Inlet Pressure Profile for λ = 3.7878E-4

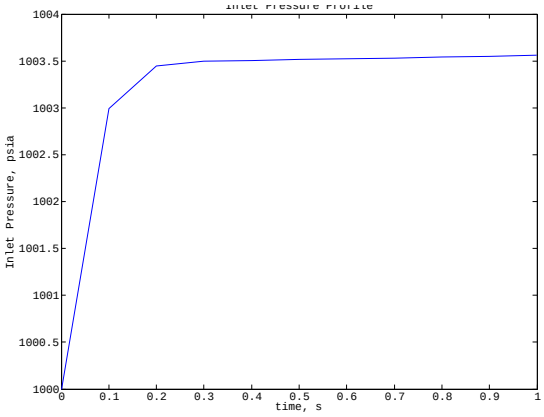

Figure C.6: Inlet Pressure Profile for λ = 3.7878E-3

Bibliography

[1] Adewumi M. A., Eltohami E. S., Ahmed W. H., "Pressure Transients Accross Constrctions," *ASME*, Vol. 122, March, 2000 pp 34–41.

[2] Adewumi M. A., Eltohami E. S., Solaja A., "Possible Detection of Multiple Blockages Using Transients," *ASME*, Vol. 125, pp. 154–159., June, 2003

[3] Ahmed W. H., "Location of partial blockage in natural gas pipelines using transient modelling", MSc. Thesis, The penn. State. U., 1996

[4] Allievi L. Teoria (Translator: Halmos, E.E), "Theory of water hammer", *American Society of Mechanical Engineering*, 1925

[5] Ametani, A., "The history of transient analysis and the recent trend", *IEEJ Trans.*, Vol. 2, pp. 497-503, 2007

[6] Angus, Robert W., "Simple Graphical Solution of Pressure Rise in Pipes and Pump Discharge Lines," *J. Eng. Inst. Canada*, Vol. 1:72, pp. 77-81, Feb. 1935

[7] Aylmer, S., "Interactive Gas Flow Analysis," Ph.D. Thesis. The University of Manchester Institute of Science and Technology, 1980.

[8] Berecz E. and Balla-Achs M., *Gas Hydrates*, Elsevier, Amsterdam, 1983

[9] Bewley L.V., *Travelling Waves on Transmission Systems* (2nd ed.), John Wiley and Sons, Inc., NY. 1951

[10] Bergeron, L., "Etude des variations de regimes dans less conduits d'eau: solution graphique generale," *Rev. Gen. Hydraul.*, Paris, Vol 1, pp. 12-25. 1935.

[11] Bucklin, R.W. ; Toy, K.G. ; Won, K.W., "Hydrate Control of Natural Gas Under Arctic Conditions Using TEG", *Proc. Gas Conditioning Conference*, 1985

[12] Carnyj, I. A., "Fundamentals of Gas Dynamics (Osnowy Gazowoy Dinamiki)," *Gostoptiehizdat*, Moscow, 1961

[13] Carnyj, I. A., "Transient Flow in Pipelines (Neustanovivsheesya Dwizheniye Realnoy Zhidkostic v Trubah)," Niedra, Moscow, 1976

[14] Chen, X. and Tsang, Y. and Zhang, H.Q. and Chen, T., "Pressure-Wave Propagation Technique for Blockage Detection in Subsea Flowlines," *SPE Annual Technical Conference and Exhibition*, 2007

[15] Chen, N.H., "An Explicit Equation for Friction Factor in Pipe," *Ind. Eng. Chem. Fundam.*, Vol 18, No. 3, pp. 296-297, 1979.

[16] Cullender, M. H., "The Isochronal Performance Method of Determining the Flow Characteristics of Gas Wells", *AIME* Vol. 204, pp. 137-142, 1955

[17] Curson, D. B. and Katz, D. L.,"Natural Gas Hydrates," *Trans. AIME*, Vol. 146, pp. 150, 1942

[18] Courant R., Friedrichs K. and Lewy H. "On the partial difference equations of mathematical physics". *IBM Journal*, pages 215–234, 1967.

[19] Crank, J. and Nicolson P., "A Practical Method for Numerical Evaluation of Solutions of Partial Differential Equations of Heat Conduction Type", Proc. Camb. Phil. Soc. 43: 5067, 1947

[20] Davidson, D. W., Gough, S. R., Ripmeester, J. A., Nakayama, H., "The Effect of Methanol on the Stability of Clathrate Hydrates" *Can. J. Chem.*, Vol. 59, pp. 2587, 1981

[21] Deaton W.M., and Frost E.M., *Gas Hydrates and Their Relation to the Operation of Natural-Gas Pipelines*, U.S. Bureau of Mines Monograph, Vol. 8, 1946

[22] Dranchuk, P. M. and Abou-Kassem, J.H., "Calculation of Z factor for Natural Gases Using Equation of State" *JCPT*, Vol 14, No. 3, pp. 34-35, July-Sept., 1974.

[23] Dendy E. Sloan, *Chlatherate hydrates of Natural Gases*, Marcel Dekker, NewYork, 1998.

[24] Eltohami E., "Modeling pressure transients in partially blocked pipelines" MSc. Thesis. The Pennsylvania State University, 1999

[25] Fetkovich, M. J., "Multipoint Testing of Gas Wells," *SPE Mid-Continent Section Continuing Education Course*, Tulsa, OK, 1975

[26] Frepoli C., Mahaffy J. H., Ohkawa K., "Notes on the implementation of a fully-implicit numerical scheme for a two-phase three-field flow model", *Nuclear Engineering and Design*, 225, pp. 191217, 2003

[27] Frepoli, C., Hochreiter, L.E., Mahaffy, J., Cheung, F.B., "A noding sensitivity analysis using COBRA-TF and the effect of spacer grids during core reflood". In: Proceedings of ICONE 8, *8th International Conference on Nuclear Engineering*, Baltimore, USA, 2000

[28] Goldwater, M.H., Rogers, K. and Turnbull, D. K., "The PAN Network Analysis Program-its Development and Use," *42nd Autumn Meeting, London, Communication 1009*, 1976

[29] Gilmore, R.E., "Lost Gas Speaking", *Gas Age-Record*, pp. 1-4, 1935

[30] Hall, G.D., Polderman, L.D., *Chem. Eng.*, Vol. 54, 52, 1960.

[31] Hammerschmidt, E. G., "Formation of Gas Hydrates in Natural Gas Transmission Lines," *Ind. Eng. Chem.*, Vol. 26, 8, pp. 851855, 1934

[32] Heath, M.J. and Blunt, J. C., "Dynamic Simulation Applied to the Design and Control of a Pipeline Network," *I.G.E Journal*, Vol 9, 4, pp. 261-274, April 1969.

[33] Hirsch, C., *Numerical computation of internal and external flows: fundamentals*, Volume 1, Elsevier, 2007

[34] Hogan D. P., "Field Results with Sonic Pinpointing", Progress report 64-D-213, presented at the 1964 A.G.A. Operating Section distribution Conf., 1964

[35] Ibraheem, S. O. and Adewumi, M. A, "Higher-Resolution Numerical Solution for 2-D Transient Natural Gas Pipeline Flows," *Presented at the Gas Technology Symposium, Calgary, Alberta Canada, SPE 35626*, Apr/May, 1996b.

[36] Issa, R. I. and Spalding, D. B., "Unsteady One-Dimensional Compressible Frictional Flow With Heat Transfer", *J. Mech. Eng. Sci.*, pp. 365369, 1972

[37] Johnsen, H. K., "Hydrates - the state of a chain reaction leading to the Piper Alpha Disaster," *Institution of Chemical Engineers Symposium Series*, No 122, pp. 1-11, 1990

[38] Kelland, M. A., Svartaas, T. M., Dybvik, L., "New Generation of Gas Hydrate Inhibitors", *70th SPE Annual Techinical Conference and Exibition*, pp. 529-537, 1995

[39] Kiuchi, T., "An Implicit Method for Transient Gas Flow in Pipe Networks", *Int. J. Heat Fluid Flow*, Vol. 15, 5, pp. 378383, 1994

[40] Koyama, H., Watanabe, K. and Himmelblau, D. M., *Identification of Partial Plugging in Gas - Transport Pipeline by ab Acoustic Method*, Applied Acoustics, Elservier Science Publishers Ltd, England, Vol. 40, 1-19, 1993.

[41] Kurganov, A. and Tadmor, E., "New High-Resolution Central Schemes for Nonlinear Conservation Laws and Convection-Diffusion Equations", *J. Comp. Phys.*, 160, 214-282, 2000

[42] Larson, D.B., "Practical use of sound amplifiers in gas leak detection", *Proc. Pacific Coast Gas Association*, 1939

[43] Larson, R. E. and Wismer, D. A., "Hierachical Control of Transient Flow in Natural Gas Pipeline Networks," *IFAC Symposium on Distribution Parameter Systems*, Banff, Alberta, Canada, 1971.

[44] Lederhos, J. P., Long, J. P., Sum, A., Christiansen, R. L., Sloan, E. D., *J. Pet. Tech.*, Vol. 51, pp. 1221, 1996

[45] Lee, A. L., Gonzales, M. H. and Eakin, B. E., "The Viscosity of Natural Gas," *Soc. Pet. Eng. SPE* 1340, Jul. 1966

[46] LeVeque, Randall J., *Finite Volume Methods for Hyperbolic Problems*, Cambridge University Press, Cambidge, UK. 2002.

[47] Lewandowski, A. and Pacut, A., "Simulation of Control Systems, (ed. I. Troch)," North-Holland, pp. 289-294, 1978

[48] Loomer, J.A. and Welch, J.W., "Some Critical Aspects of Designing for High Dewpoint Depression with Glycols", *Proc. Gas Cond. Conf.*, 1961

[49] Loth J. L., Morris G. J., Palmer G. M., Guiler R., Mehra D., "Acoustic Detecting and Locating Gas Pipe Line Infringement", *National Energy Technology Laboratory Strategic Center For Natural Gas (SCNG)*, 2004

[50] Makogon, Y.F., *Hydrates of Natural Gas*, Moscow, Nedra, Isadatelstro, 208, (Translated from Russian (1981) by W.J. Cieslesicz,PennWell Books, Tulsa, Oklahoma, p.237)

[51] Manning, F.S. and Thompson, R.E., *Oilfield Processing of Petroleum: Natural Gas, Volume 1*, Pennwell Publishing Company, Tulsa, Oklahoma, 1991.

[52] McCain W.D., *The Property of Petroleum Fluids*, Technology and Engineering, PenWell Publishing, Tulsa, Oklahoma. 1990

[53] McElwee, "The Sonic Leak detector", *Am. Gas J.*, 184, pp. 14-17, 1957

[54] Nakayama, H. and Hashimoto, M., *Bull. Chem. Soc. Japan*, pp. 2427, 1980

[55] Nessyahu, H. and E. Tadmor , "Non-oscillatory central differencing for hyperbolic conservation laws", *J. Comp. Phys.*, 87, pp. 408463, 1990.

[56] Osiadacz, A.J.,"Optimal Numerical Method of Simulating Dynamic Flow of Gas in Pipelines," *Int. J. Num. Fluids*, Vol 3, pp. 125 - 35, 1983a.

[57] Osiadacz, A.J., *Simulation and Analysis of Gas Networks*, Gulf Publishing Company, Houston, Texas, 1987.

[58] Parker, John, "Acoustic Detection and Location of Leaks in Underground Natural Gas Distribution Lines", *John Hopkins APL Technical Digest*, Vol. 2, pp. 90-101, 1981

[59] Parmakian, J., *Water - Hammer Analysis*, Dover New York, 1963.

[60] Perry, C.R., *Oil and Gas Journal*, Vol. 58, 71, 1960

[61] Poloni, M., Winterbone, D. E., and Nichols, J. R., "The Calculation of Pressure and Temperature Discontinuity in a Pipe by Method of Characteristics and the Two-Step Differential Lax-Wendroff Methods", *ASME FED*, Vol. 62, pp. 1-7, 1987

[62] Rachford, H. H., and Dupont, T. A., "A Fast, High Accurate Means of Modelling Transient Flow in Gas Pipeline Systems by Variational Mthods," *Soc. Pet. Eng. J., SPE 4005A, Trans. AIME*, Vol. 257, pp. 165-178, April 1974

[63] Reid, J. M., Hogan D.P. and Michel P. L., "A New Approach to Pinpointing Gas Leaks with Sonics", *presented at the 1961 A.G.A. Operating Section Distribution Conference.*, 1961

[64] Richardson, R.B., "Listening for leaks", *Gas Age-Record*, 1935

[65] Schnyder O., "Druckstosse in Pumpensteigleitungen", *Druckstosse in Pumpensteigleitungen*, Vol. 94(22):271, 1929

[66] Scott, S.L. and Satterwhite, L.A., "Evaluation of the Backpressure Technique for Blockage Detection in Gas Flowlines",*J. of Energy Resources Technology*, 120, 27. March, 1998

[67] Sharp, D.B. and Campbell, D.M. "Leak Detection in Pipes Using Acoustic Pulse Reflectometry," *EPSRC Report*, 1-14, 1996

[68] Sloan, E.D., *Clathrate Hydrates of Natural Gases*, Marcel Dekker, 1990

[69] Sloan B., *J. Pet. Tech.* 1414, December 1991

[70] Svatas, T.M. ,Fadnes,F.H., Proceedings *Intl. Offshore and Polar Eng. Conf.* 614, June 1992

[71] Smith, O. L., "The Soundograph System for Gas Leak Detection", *Gas Age-Record*, pp. 381-383, 1933

[72] Sod, G. A., "A Survey of Several Finite Difference Methods for Systems of Nonlinear Hyperbolic Conservation Laws," *J. Computational Physics*, Vol 27, pp. 1, 1978.

[73] Stoner, M. A., "Analysis and Control of Unsteady Flows in Natural Gas Piping Systems," *ASME, D.J. Basic. Eng.*, Vol. 91, pp. 331-340, Sept. 1969.

[74] Streeter, V. L. and Wylie, E. B., "Natural Gas Pipelines Transients," *Soc. Pet. Eng. J.*, *SPE 2555*, pp. 357-364, Dec, 1970.

[75] Taylor, T. D., Wood, N. E. and Powers, J. E. , "A Computer Simulation of Gas Flow in Long Pipelines," *Soc. Pet. Eng. J.*, Vol 10, pp.357-364, 1962.

[76] Thomas, L. K., Hankinson, R. W. and Philips, K. A. , "Determination of Acoustic Velocities for Natural Gas," *J. Pet. Tech.*, Vol. 22, pp. 889-895, 1970.

[77] Tian. S. and Adewumi, M. A.," Development of Analytical Design Equation for Gas Pipelines," *SPE Prod. And Fac. J.*, pp. 100-106, May, 1994

[78] Tiratsoo, J. N. H., *Pipeline Pigging Technology*, 2nd Edition, Gulf Publishing Company, 1992.

[79] Thompson, W.C. and Skogman, K.D. "Application of Real Time Flow Modeling to Pipeline Leak Detection" *J. of Energy Resources Tech.,transactions of ASME*, Vol. 105, 4, pp. 536-541, 1983

[80] Van Leer, B., "Towards the ultimate conservative difference scheme III. Upstream-centered finite-difference schemes for ideal compressible flow", *J. Comp. Phys.*, 23, pp. 263-275, 1977

[81] Van Leer, B., "Towards the Ultimate Conservative Difference Scheme, V. A Second Order Sequel to Godunov's Method", *J. Com. Phys.*, 32, pp. 101-136, 1979

[82] Van Leer, B., "Flux-Vector Splitting for Euler Equations," *ICASE Report* 82-30, (1982).

[83] Watanabe, K. and Himmelblau, D. M., "Detection and Location of a Leak in a Gas- transport pipeline by a new acoustic method," *AIChE J.*, Vol 32, No. 10, pp.1690-1701, 1986

[84] Watanabe, K., "Location of a leak in al long gas-transport pipeline by the acoustic method," *Soc. Of Instruments and Control Engineers (Japan) Trans.*, Vol 23, No. 2, 1987

[85] Watanabe, K. Koyama, H. and Ohno, H., "Location of a leaks in gas - transport pipeline by a the acoustic method," *Proc. Of International Soc. Of America (ISA)/87. Int. Conf. and Exch., ISA*, pp. 619-26, 1987.

[86] Watanabe, K. and Koyama, H., "Location and Estimation of a pipeline leak," *Electrical Engng. In Japan*, Vol. 110, No. 7, pp. 92-101, 1990

[87] Wilkinson, J. F., Haliday, D. V., Batey, J. F. and Hannah, K. W., *Transient Flow in Natural Gas Transmission Systems*, AGA, New York, 1965.

[88] Wylie, E. B. Streeter, V. L and Stoner, M. A., "Unsteady-State Natural - Gas Calculations in Complex Pipe Systems, " *Soc. Pet. Eng. J., AIME*, Feb. 1974

[89] Wylie, E. B. and Streeter, V. L., *Fluid Transients in Systems*, Prentice Hall, 1993

[90] Wylie, E. B., Stoner, M. A., and Streeter, V. L., "Network System Transient Calculation by Implicit Method", *Soc. Pet. Eng. J.*, Vol. 11, pp. 356362, 1971

[91] Yow, W., "Numerical Error in Natural Gas Transient Calculations," Ph.D. Dissertation University of Michigan, Ann Harbor, 1972

[92] Zhou, J. and Adewumi, M. A., "Simulation of Transients in Natural Gas Pipelines Using TVD schemes," *Int. J. for Numerical Methods in Fluids* 1995

[93] Zhou, J. and Adewumi, M. A., "Simulation of Transients in Natural Gas Pipelines," *SPE Production & Facilities*, 1996

[94] Ziolko, M., "Dynamic Optimization of a Natural Gas Pipeline," Ph.D. Thesis, Stanislaw Staszic Academy of Mining and Metallurgy, Cracow, (1973).